

GeFL: Model-Agnostic Federated Learning with Generative Models

Honggu Kang, Seohyeon Cha, Joonhyuk Kang

Abstract—Federated learning (FL) is a promising paradigm in distributed learning while preserving the privacy of users. However, the increasing size of recent models makes it unaffordable for a few users to encompass the model. It leads the users to adopt heterogeneous models based on their diverse computing capabilities and network bandwidth. Correspondingly, FL with heterogeneous models should be addressed, given that FL typically involves training a single global model. In this paper, we propose *Generative Model-Aided Federated Learning* (GEFL), incorporating a generative model that aggregates global knowledge across users of heterogeneous models. Our experiments on various classification tasks demonstrate notable performance improvements of GEFL compared to baselines, as well as limitations in terms of privacy and scalability. To tackle these concerns, we introduce a novel framework, GEFL-F. It trains target networks aided by *feature-generative models*. We empirically demonstrate the consistent performance gains of GEFL-F, while demonstrating better privacy preservation and robustness to a large number of clients. Codes are available at [1].

Index Terms—Federated learning, model heterogeneity, generative model, data augmentation.

I. INTRODUCTION

DEEP learning has demonstrated remarkable success across various domains, due to the availability of abundant training data. However, with the proliferation of edge devices like mobile and Internet-of-Things (IoT) devices, which generate substantial amounts of decentralized data, there arises a challenge in effectively aggregating distributed information and collaboratively training neural networks. Federated learning (FL) is a promising solution, facilitating collaborative model training by leveraging data from multiple clients while preserving privacy without sharing client’s raw data. In FL, the server collects knowledge (e.g., model weights) from clients and subsequently aggregates it to make clients share the global knowledge [2]. Many recent studies have explored such potential of FL in many practical applications [3], [4].

Simultaneously, the increasing growth rate of model size [5]–[7] and the growing heterogeneity of edge devices [8] pose additional challenges in FL. Edge devices exhibit diverse capabilities, encompassing factors such as computing power, memory, and communication environment. Given the

limitations of edge devices to accommodate large models beyond their capabilities, the necessity arises for these devices to adopt personalized and optimized heterogeneous model architectures.

However, many FL algorithms aim to train a *single global model* [2], [9], creating a challenge for devices with personalized model architectures when collaboratively training their models with others having different architectures. Hence, there needs a solution to aggregate knowledge from edge devices, even when clients have heterogeneous models. While there have been studies on training multiple models in FL [3], [10], [11], previous approaches typically involve scaling down a global model into smaller submodels. Consequently, a client with a model that is not a subset of the global model cannot be trained within the same FL framework. Different lines of work have proposed the incorporation of additional public data through assembly to address model heterogeneity [12]–[15]. However, these approaches necessitate access to a well-curated public dataset in either clients or the server.

In this paper, we introduce *Generative model-aided Federated Learning* (GEFL), a framework that addresses the challenge of training multiple models with diverse architectures tailored to the heterogeneous requirements of individual clients (e.g., memory, computing, and bandwidth dynamics). GEFL incorporates a *federated generative model*¹ trained in a federated manner on clients’ local data. This generative model augments local training data by generating synthetic samples for the training of heterogeneous models [16]. However, training a generative model in a distributed manner poses challenges, especially when dealing with a large number of clients, leading to issues such as mode collapse, blurry, and low-quality generated images [17]–[19]. Moreover, the trained generative model may conflict with the privacy-preserving benefits of FL. Therefore, we propose GEFL-F, which employs generative models that produce *features*, which are the output of a common feature extractor within heterogeneous models. Our proposed algorithm effectively aggregates global knowledge from feature-generative models under model-heterogeneity, while mitigating related to generative model training and privacy concerns.

The main contributions of this paper are summarized as follows:

- We propose GEFL, an algorithm for FL with clients of heterogeneous model architectures employing generative models.

¹Employing a federated generative model improves the performance, though training a generative model could burden the clients.

Manuscript received XXX, XX, 2024; revised XXX, XX, 2024; accepted XXX, XX, 2024. Recommended for acceptance by Dr. X. (Honggu Kang and Seohyeon Cha contributed equally to this work.)

H. Kang is with Samsung Electronics, Suwon 16677, South Korea. (e-mail: honggu.kang@samsung.com).

S. Cha is with the University of Texas at Austin, TX 78712, USA (e-mail: seohyeon.cha@utexas.edu)

J. Kang is with the School of Electrical Engineering, Korea Advanced Institute of Science and Technology (KAIST), Daejeon 305-701, South Korea. (e-mail: jhkang@ee.kaist.ac.kr).

TABLE I: Summarization of main notations

| Symbol | Definition |
|------------------|--|
| \mathcal{C} | Client set in each round |
| T_{KA} | Number of FL communication rounds for training generative model |
| T_{TN} | Number of FL communication rounds for training target networks |
| T_{FE} | Number of FL communication rounds for training feature extractor |
| T_g | Number of local epochs for training generative model |
| T_s | Number of local epochs for training target networks by synthetic samples |
| T_r | Number of local epochs for training target networks by real samples |
| T_w | Number of local epochs for warming up common feature extractor |
| \mathbf{w}_g | Global weights of generative model |
| \mathbf{w}_k | Local weights of generative model of client k |
| x, y | Data sample from a dataset |
| x^{feat}, y | Feature sample from a feature generative model |
| B | Batch size |
| \mathcal{D}_k | Local dataset of client k |
| M | Number of heterogeneous models |
| $\theta_{g,m}$ | Global weights of m -th target model |
| $\theta_{k,m}$ | Local weights of m -th target model of client k |
| θ_g^f | Global weights of common feature extractor |
| $\theta_{g,m}^h$ | Global weights of header of m -th target model |
| $F(\cdot)$ | Feature extractor model |
| $G(\cdot)$ | Federated generative model |
| $J_G(\cdot)$ | Loss function for training generative model |
| $J(\cdot)$ | Loss function for training target networks |
| α | Learning rate for training target networks |
| β | Learning rate for training a generative model |

- We study the effectiveness of federated generative models in terms of downstream performance, privacy, and scalability.
- We propose GEFL-F, an improved version of GEFL, employing feature-generative models to address privacy and scalability, while maintaining performance gains from generative models.

The remainder of this paper is organized as follows. Section II briefly reviews related works and we present our proposed method, GEFL in III. Then, we introduce GEFL-F in Section IV. Section V presents the insights obtained in experimental results and Section VI concludes the paper. Detailed experimental settings are presented in [1].

II. RELATED WORKS

A. Federated learning

FL trains models while data is distributed across multiple clients. Most approaches involve training a *single* global model [2], [9], [20] and the foundational algorithm, FedAvg [2] gathers global knowledge at the server by aggregating the model parameters from clients and averaging them. Another line of work integrates knowledge distillation (KD) [21] into FL to transfer knowledge from client models to the server model [12], [22]–[24]. For example, FedKD [23] shares a

small student model while keeping a local teacher model at each client to reduce communication costs. FedDKD [24] addresses data heterogeneity across clients by averaging the knowledge of clients by KD. However, none of these works specifically aim to address model heterogeneity.

B. Model heterogeneous FL

To address model heterogeneity in FL, several approaches have proposed scaling a global model into submodels in widthwise [10], [25], in depthwise [11], and both widthwise and depthwise [3]. However, these methods scale the model into a subset of the global model, requiring all clients to share the same model architecture. Our proposed method allows for the training of heterogeneous models with different architectures across clients.

Another approach tackles model heterogeneous FL by leveraging the concept of ensembling various models. AvgKD [4] requires a client to receive all other models from other clients and compute an averaged logit of all logits from local samples of these models. However, this can be computationally infeasible with a large number of clients and less effective when models across clients have significant architectural differences. In addition to the above techniques, some studies introduce architectural conditions such as training a common extractor [26] or sharing additional model [27].

Recent studies have proposed to incorporate additional public data to enhance ensembling methods for addressing model heterogeneity [12]–[15]. For instance, FedDF [12] conducts ensemble distillation between the client and global models, utilizing synthetic data from a pre-trained generator or unlabeled public data. FCCL [13] incorporates unlabeled datasets by introducing a loss term defined on logits of unlabeled public data and the averaged logit across clients. FedMD [14] leverages labeled public data for transfer learning through knowledge distillation. pFedHR [28] has the flexibility to leverage either labeled or unlabeled public data. However, these algorithms often require access to a well-curated public dataset in either clients or the server, which does not exist in practical for real-world training. Instead, our framework employs existing local data in each client.

C. Generative models in FL

Several works have delved into FL by incorporating generative models, such as VAE [29] and GAN [30]. FedGAN [31] investigates the federated training of GANs, while other studies involve training a generator supervised by a well-trained model to address statistical heterogeneity when training a single model [32], [33]. In previous studies, generative models could not be effectively trained when client models were heterogeneous, limiting their applicability. In contrast, our approach enables generative models to be trained collaboratively, even in the presence of heterogeneous client models. Furthermore, existing methods often fail to significantly enhance generalization, as the generator tends to produce samples that only reinforce the existing capabilities of well-trained models. While FedCG [34] adopts a similar technique by employing a conditional GAN to generate intermediate features, it does not

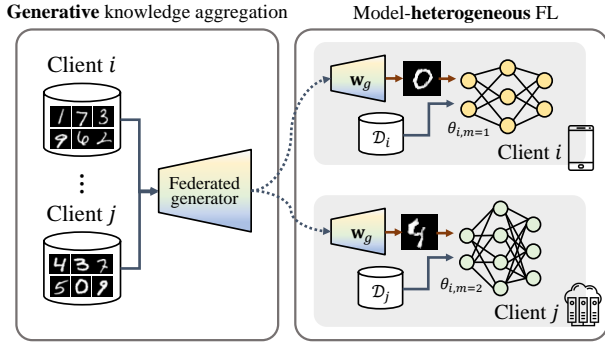


Fig. 1: **Illustration of GeFL.** We propose a model-agnostic FL framework under model-heterogeneity, GEFL, consisting of (i) *generative knowledge aggregation* which trains a generative model in a federated manner, and (ii) *heterogeneous target network training* augmented by trained generative models.

explicitly tackle model heterogeneity as our approach does. Additionally, FedCG relies on sharing a classifier between clients and the server, whereas our method, GEFL-F, uniquely shares only the feature extractor, addressing both model and statistical heterogeneity.

III. GENERATIVE MODEL-AIDED MODEL HETEROGENEOUS FL

A. Framework

To address the model heterogeneity in FL, GEFL incorporates a conditional generative model trained in a federated manner using local clients' data, as illustrated in Figure 1. GEFL consists of two main processes: (i) federated generative model (FedGen) training for *global knowledge aggregation* and (ii) *target network training* augmented by generative models (see Algorithm 1 for details).

In the generative knowledge aggregation stage, generative models are trained to capture the representation of real samples. Each client $k \in \mathcal{C}$ trains a generative model G with parameters \mathbf{w}_k using its local data. The server then aggregates the generative model parameters as $\mathbf{w}_g \leftarrow \frac{1}{|\mathcal{C}|} \sum_{k \in \mathcal{C}} \mathbf{w}_k$ and sends them back to each client for the next round.

The trained generative model effectively gathers global knowledge from every client, enabling the training of target networks despite the different model architectures among clients. Specifically, we assume that each client has a model architecture with an index $m \in \{1, \dots, M\}$ for their target network, where there exist M candidate heterogeneous architectures (e.g., different CNNs or the combination of ResNet [35], EfficientNet [36], and MobileNet [37]).

Then, during target network training and refinement, target networks are updated by forwarding synthetic samples and real samples separately. In each round of target network training, each client k trains its target network $T_{\theta_{k,m}}$ using samples generated by FedGen $G(\cdot|y_i, \mathbf{w}_g)$ conditioned on random label $y_i \sim p(y)$, treating them as augmented training samples for multiple local epochs as

$$\min_{\theta_{k,m}} \mathbb{E}_{z_i, y_i \sim \mathcal{N}(\mathbf{0}, \mathbf{I}), p(y)} [\text{CE}(\rho(T_{\theta_{k,m}}(G(z_i|y_i, \mathbf{w}_g))), y_i)],$$

Algorithm 1 GeFL framework enabling model heterogeneous FL using federated generative models.

(i) **generative knowledge aggregation**
for each round $t = 1, 2, \dots, T_{KA}$ **do**
 GeFL server broadcasts \mathbf{w}_g to clients.
for all client $k \in \mathcal{C}$ in parallel **do**
 Initialize local parameters $\mathbf{w}_k \leftarrow \mathbf{w}_g$
for $t = 1, \dots, T_g$ **do**
 $\{(x_i, y_i)\}_{i=1}^B \sim \mathcal{D}_k$
 $\mathbf{w}_k \leftarrow \mathbf{w}_k - \beta \nabla_{\mathbf{w}_k} J_G(\mathbf{w}_k)$
 Client k sends \mathbf{w}_k to the server
 $\mathbf{w}_g \leftarrow \text{Agg}(\{\mathbf{w}_k\}_{k \in \mathcal{C}})$ \triangleright Algorithm 2 (Aggregate)

(ii) **target network training**
for each round $t = 1, 2, \dots, T_{TN}$ **do**
 GeFL server multicasts $\{\theta_{g,m}\}_{m=1}^M$ to clients.
for all client $k \in \mathcal{C}$ in parallel **do**
 Initialize local parameters $\theta_{k,m} \leftarrow \theta_{g,m}$
for $t = 1, \dots, T_s$ **do**
 $\{(x_i, y_i)\}_{i=1}^B \sim G(z_i|y_i, \mathbf{w}_g)$
 $\theta_{k,m} \leftarrow \theta_{k,m} - \alpha \nabla_{\theta_{k,m}} J(\theta_{k,m})$
for $t = 1, \dots, T_r$ **do**
 $\{(x_i, y_i)\}_{i=1}^B \sim \mathcal{D}_k$
 $\theta_{k,m} \leftarrow \theta_{k,m} - \alpha \nabla_{\theta_{k,m}} J(\theta_{k,m})$
 $\theta_{g,m} \leftarrow \text{Agg}(\{\theta_{k,m,k}\}_{k \in \mathcal{C}, m_k=m}), \forall m \in \{1, \dots, M\}$

Algorithm 2 Aggregate

Input: set of model parameters $\{\theta_k\}_{k \in \mathcal{C}_{\text{agg}}}$ with the same architecture
 $\theta_g \leftarrow \frac{1}{|\mathcal{C}_{\text{agg}}|} \sum_{k \in \mathcal{C}_{\text{agg}}} \theta_k$
Return θ_g

where ρ is the softmax function and CE is the cross-entropy function. After training target networks on generated samples from G , the target networks are trained on real data samples subsequently. In our algorithm, trained FedGens offer diverse training synthetic samples, contributing to overcoming model heterogeneity in FL. The learning rates are α for the generative model G and β for the target networks.

B. Evaluation of GeFL

a) *Experimental settings:* We assessed the performance of GeFL on three public datasets: MNIST [38], Fashion-MNIST [39] (FMNIST in short over the paper), and CIFAR10 [40]. For MNIST and FMNIST with 1-channel images, our heterogeneous target networks comprise ten different convolutional neural networks (CNNs). For evaluating datasets of 3-channel images, we employ different set of CNNs with CNNs employed for 1-channel images². The model architectures of ten networks are detailed in Appendix [1]. The number of clients is 10 ($|\mathcal{C}| = 10$) unless otherwise noted. The other hyperparameters used in training target networks and

²We also conducted experiments with different set of model architectures (eight EfficientNet [36] backbones and two with ResNet [35] backbones) and the results showed the similar tendency.

generative models are presented in Appendix (Table IX and Table X) [1]. Our baseline methods consist of 5 relevant FL approaches: two from homogeneous FL, FedAvg [2], FedProx [9], and three from heterogeneous FL, AvgKD [4], FedDF [12] and LG-FedAvg [26].

b) Comparison to FL baselines: The performance of GEFL under model heterogeneity with different types of generative models is detailed in Table II. We use the prefix *Fed* to indicate the type of generative model trained in a federated manner and employed for augmenting target network training. The performance was evaluated based on the mean classification accuracy (%) across 10 heterogeneous target networks throughout the paper.

GEFL *with all types of generative models outperformed other baselines in scenarios where all clients’ models have different architectures.* While AvgKD³ allows flexibility in client model architectures, it resulted in lower accuracy than FedAvg on FMNIST and CIFAR10, attributed to its use of averaged logits from clients’ models as pseudo-labels, even when some of the models were not adequately trained. The training process of FedDF involved aggregating logits on a public dataset obtained from trained target networks. However, the performance of FedDF was notably sensitive to the choice of public dataset. We used the public dataset SVHN for MNIST, CIFAR10 for FMNIST, and CIFAR100 for the CIFAR10 dataset. When the training data and the chosen public dataset exhibit considerable dissimilarities in distribution (e.g., FMNIST and CIFAR10), FedDF failed to achieve comparable performance. Furthermore, although LG-FedAvg exhibits improvements over FedAvg, it requires a common feature extractor and is not applicable to completely heterogeneous settings. In contrast, GEFL consistently showed improvements, benefiting from global knowledge obtained from federated generative models.

c) Different generative models: Generative models learn to capture the representation of training data, aiming to generate samples that adhere to the training data distribution. The essential attributes expected from generative models include high-quality sampling, high sample diversity, and fast (computationally inexpensive) sampling. Notable generative models we use have different strengths and weaknesses as follows. Generative Adversarial Networks (GANs) [17], [41] provide high-quality and fast sampling but are prone to mode collapse. Variational Autoencoders (VAEs) [18], [42] offer fast and diverse sampling, albeit with lower sample quality. Denoising diffusion probabilistic models (DDPMs) [19], [43] deliver diverse and high-quality sampling at the cost of being computationally expensive. Note that w denotes the guidance score for diffusion models [44].

Referring to Table III, the performance gain (over FedAvg) of GEFL varies across generative models, with no clear correlation between Fréchet Inception Distance (FID) score [45]

³We present the highest performance of AvgKD within a few initial rounds (approximately 30 rounds), as the accuracy rapidly decreases thereafter due the significant heterogeneity in our setting.

⁴To evaluate the performance, we conducted training of both FedGens and target networks using varying proportions of the complete dataset (detailed in Table IX). The observed performance improvements differs by the amount of data utilized in the training process.

| Method | MNIST | FMNIST | CIFAR10 |
|--------------------------------|--------------|--------------|--------------|
| FedAvg [2] | 92.62 | 80.58 | 55.65 |
| FedProx [9] | 92.57 | 80.50 | 55.10 |
| AvgKD [4] | 92.81 | 77.12 | 26.36 |
| FedDF [12] | 91.39 | 58.81 | 57.17 |
| LG-FedAvg [26] | 92.71 | 80.61 | 54.49 |
| GEFL (FedDCGAN) | 95.32 | 83.11 | 58.45 |
| GEFL (FedCVAE) | 94.46 | 82.33 | 55.80 |
| GEFL (FedDDPM _{w=0}) | 96.44 | 82.43 | 59.36 |
| GEFL (FedDDPM _{w=2}) | 95.17 | 81.51 | 58.47 |

TABLE II: Mean classification accuracy⁴(%) evaluation of GEFL on the MNIST, FMNIST, and CIFAR10 dataset

| Dataset | Model | FID↓ | IS↑ | Perf. gain↑ | MND↓ |
|---------|------------------------|--------------|-------------|-------------|--------------|
| MNIST | FedDCGAN | 7.83 | 1.56 | 2.7 | 1.035 |
| | FedCVAE | 41.41 | 1.55 | 1.84 | 0.714 |
| | FedDDPM _{w=0} | 77.71 | 1.77 | 3.82 | 0.640 |
| | FedDDPM _{w=2} | 73.40 | 1.60 | 2.55 | 0.753 |
| FMNIST | FedDCGAN | 31.55 | 2.13 | 2.53 | 0.994 |
| | FedCVAE | 79.87 | 1.86 | 1.75 | 0.553 |
| | FedDDPM _{w=0} | 138.41 | 2.41 | 1.85 | 0.119 |
| | FedDDPM _{w=2} | 82.00 | 2.18 | 0.93 | 0.135 |
| CIFAR10 | FedDCGAN | 23.44 | 4.13 | 2.8 | 0.979 |
| | FedCVAE | 125.60 | 2.92 | 0.15 | 0.502 |
| | FedDDPM _{w=0} | 66.99 | 3.79 | 3.71 | 0.842 |
| | FedDDPM _{w=2} | 53.38 | 3.25 | 2.82 | 0.808 |

TABLE III: Evaluation of federated generative models where neither FID nor IS exhibits a clear connection to the performance of GEFL. MND here represents the mean nearest neighbor distance ratio, with the value indicating severe memorization if they are larger than 1 on average, as explained in Section III-C.

| Method | FedAvg | GEFL (FedDCGAN) |
|------------------|------------|--------------------|
| None | 55.65±0.68 | 58.45±0.49 |
| MixUp [47] | 60.07±1.13 | 62.67 ±0.24 |
| CutMix [48] | 58.95±0.61 | 61.66±0.41 |
| AugMix [49] | 53.96±0.37 | 56.47±0.25 |
| AutoAugment [50] | 56.99±0.43 | 59.97±0.38 |

TABLE IV: Mean classification accuracy (%) of GEFL combined with data augmentation on the CIFAR10 dataset

and Inception Score (IS). This aligns with recent findings suggesting that FID and IS metrics do not reliably predict downstream performance [46]. The rationale is that while generated samples introducing diversity to the local real data can enhance performance, excessively degraded samples, which deviate significantly from the real data distribution, can negatively impact the results. This highlights the importance of evaluating GEFL holistically, rather than focusing solely on generative model performance. In general, GANs and diffusion models demonstrate strong GEFL performance. However, GANs tend to be sensitive to hyperparameter selection, whereas diffusion models incur significantly higher computational costs during sample generation.

d) Comparison to data augmentation: We conducted a performance comparison of GEFL to existing data augmentation (DA) methods. DA is a widely used technique to enhance

the generalization performance, particularly in scenarios with limited training data [47]–[50]. Note that DA and GEFL are orthogonal, meaning they can be combined to achieve even greater performance gains.

To show the effectiveness of GEFL in such scenarios, we provide comparison to MixUp [47], CutMix [48], AugMix [49], and AutoAugment [50] in Table IV. Here, we used GEFL with FedDCGAN which shows improved accuracy with reasonable computational complexity. Notably, GEFL combined with DA yielded further performance improvements. While DA augments local samples independently at each client, given the inability to share raw data with other clients, GEFL utilizes a generative model with global knowledge across all clients to generate synthetic samples, utilizing more diverse samples than local samples. Throughout the paper except Table IV, to provide a focused evaluation of GEFL, we assessed its performance without incorporating DA.

C. Discussions and limitations

a) *Privacy concerns*: While generative models present a promising solution to address model heterogeneity, sharing them between clients and the server introduces significant privacy concerns. Note that, although not sharing target networks alleviates model inversion attacks [51], [52], privacy issues persist due to the sharing of a generative model trained on the global data distribution of all clients. This is particularly concerning with the recent emergence of privacy threats, called *memorization* [53]–[56], where the generative model creates images that resemble training samples.

In this work, the memorization of federated generative models is assessed by the averaged *mean nearest neighbor distance (MND) ratio*, as indicated in Table III. The MND ratio is defined as

$$\mathbb{E}[\rho_i], \text{ where } \rho_i = \frac{\min_{\mathbf{x} \in \mathcal{V}} d(\mathbf{x}_i, \mathbf{x})}{\min_{\mathbf{x} \in \mathcal{S}} d(\mathbf{x}_i, \mathbf{x})}$$

indicates the ratio between the minimum distance from a training sample x_i to the nearest synthetic sample set and the minimum distance from the training sample to the nearest validation sample set [53]. \mathcal{S} represents the set of synthetic samples from a generative model, \mathcal{V} denotes the validation set with same cardinality ($|\mathcal{S}| = |\mathcal{V}| = 600$). Here, we used the perceptual metric, LPIPS (learned perceptual image patch similarity) [57] to measure the distance $d(\cdot, \cdot)$, that is the similarity between samples⁵ and were averaged over 1000 \mathbf{x}_i samples. Note that if ρ_i is larger than 1, it indicates that the real training sample \mathbf{x}_i is more similar to generated samples than the real validation samples and vice versa for ρ_i is less than 1.

b) *Scalability across the number of clients*: FL often struggles with distributed data, as an increase in distributed data causes greater divergence in gradients. GEFL also shows the vulnerabilities to the distributed data. Figure 4 demonstrates that as the number of clients increases, both performance and the gain of GEFL compared to baseline decreases.

⁵LPIPS captures image similarity as human perception, in contrast to traditional metrics like Euclidean distance.



Fig. 2: Generated images from FedCVAE (top two rows) and FedDCGAN (bottom two rows) which are trained across the different number of clients⁶

It is due to the reduced quality of generated samples from federated generative models as Figure 2. As the same amount of real datasets is distributed to more clients, the quality of images diminishes. This is attributed to the increased difficulty in achieving convergence during training a federated generative model over a larger number of clients [58].

Table V provides a detailed comparison of the parameter sizes and computational costs associated with various generative models in GEFL, with the goal of understanding their efficiency and resource demands. The total parameters include all the components of each model that are essential for the operation of the models, such as the generator and discriminator in FedDCGAN and the encoder and decoder in FedCVAE. It is also important to note that the number of parameters directly impacts the communication cost, as participating clients must transmit these parameters to the server. On the other hand, the generator parameters refer specifically to the components directly involved in the image generation process—for example, the generator in FedDCGAN or the decoder in FedCVAE. This distinction provides a more precise understanding of the resources allocated specifically to the generation process.

The computational costs are divided into two categories: training cost and sampling cost. The training cost, measured in multiply-accumulate operations (MACs), reflects the computational expense of training all components of the generative model per epoch. The sampling cost, also measured in MACs, is limited to the resources required for generating images. It is worth noting that the sampling cost for FedDDPM is significantly higher compared to the other models. This is because FedDDPM employs a diffusion process that generates images through a series of time steps, resulting in a sampling cost proportional to the number of these steps. Consequently, the sampling cost for FedDDPM is calculated as the training cost multiplied by the total number of time steps.

These analyses underscore the importance of evaluating model gain, privacy considerations, computational cost, and communication cost when selecting an appropriate generative model for GEFL.

⁶Throughout the paper regarding experiments on the number of clients, note that the same amount of dataset is distributed over the varying number of clients. For example, each client has 60 samples for the client number 100, while each client has 600 samples for the client number 10.

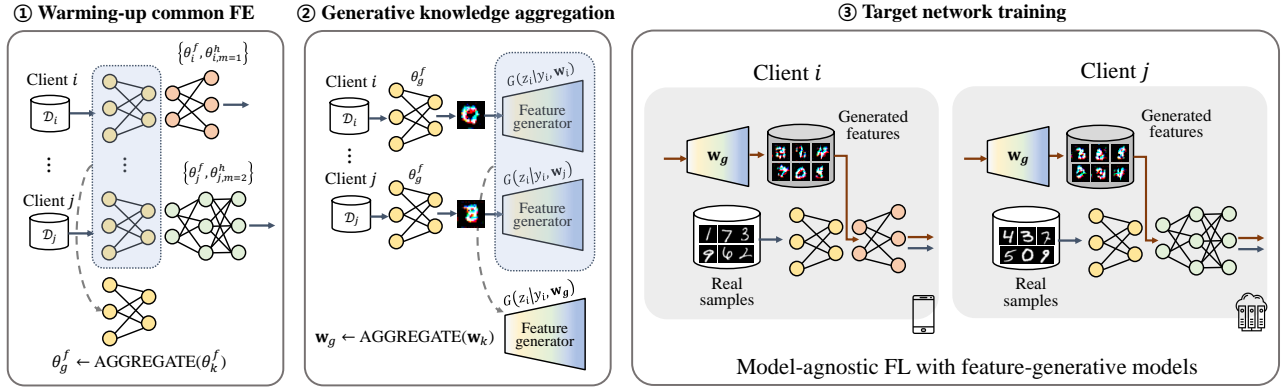


Fig. 3: **Illustration of GEFL-F algorithm.** Each target network is decoupled into a common feature extractor and a heterogeneous header. There are three main stages in GEFL-F including (i) *warming-up phase* for training a common feature extractor, and (ii) *generative knowledge aggregation* which trains feature-generative models using warmed-up feature extractor, and (iii) *target network training*, especially the heterogeneous headers, using real samples and generated features.

| | FedDCGAN | FedCVAE | FedDDPM |
|----------------------|----------|---------|---------|
| # Total Params. | 5.72M | 22.35M | 7.569M |
| # Generator Params. | 3.077M | 11.17M | 7.569M |
| Training Cost (MACs) | 347.74M | 169.41M | 2.21G |
| Sampling Cost (MACs) | 277.74M | 135.29M | 220.87G |

TABLE V: Cost comparison of generative models in GEFL

IV. FEATURE GENERATIVE MODEL-AIDED FL

In this section, we introduce GEFL-F, a novel framework designed to address the challenges posed in GEFL, including privacy preservation, scalability, and communication efficiency. This leverages feature-generative models to tackle these issues effectively. We use the suffix *-F* to indicate the feature-generative models (e.g., FedDCGAN-F, FedCVAE-F).

Our primary motivation is to design a lightweight federated generative model that preserves privacy on training data of individual clients while simultaneously aggregating global knowledge to benefit the training of heterogeneous networks. To achieve this, we incorporate feature-generative models that are trained on features, which represent the output of a common feature extractor comprising a few layers of the target network. Given the lower resolution of features compared to the original images, sharing feature-generative models offers a potential to mitigate privacy concerns [51], [59], [60], and further reduces the required size of generative models to learn a global knowledge [61]. As information passes through the successive layers of a convolutional layers, the focus shifts from fine-grained pixel-level details to more abstract, high-level features. This process results in a trade-off: while high-level semantic content is preserved and enhanced, detailed pixel information is progressively discarded or generalized [51], [62]. These findings motivate the inherent design of feature extract to prioritize semantic understanding, which is advantageous for preserving privacy.

A. Framework

An overview of GEFL-F is provided in Figure 3. Each client has its target network from M candidate models, each consist-

Algorithm 3 GEFL-F framework enabling model heterogeneous FL using federated feature-generative models.

(i) *warming-up common feature extractor*

for each round $t = 1, 2, \dots, T_{FE}$ **do**
The server multicasts $\{\theta_g^f, \theta_{g,m}^h\}_{m=1}^M$ to clients.

for each client $k \in \mathcal{C}$ in parallel **do**

Initialize local parameters $\theta_{k,m} \leftarrow \theta_{g,m}$

for each local epoch $t = 1, \dots, T_w$ **do**

$\{(x_i, y_i)\}_{i=1}^B \sim \mathcal{D}_k$

$\theta_{k,m} \leftarrow \theta_{k,m} - \alpha \nabla_{\theta_{k,m}} J(\theta_{k,m})$

$\theta_g^f \leftarrow \text{Agg}(\{\theta_k^f\}_{k \in \mathcal{C}})$

$\theta_{g,m}^h \leftarrow \text{Agg}(\{\theta_{k,m,k}^h\}_{k \in \mathcal{C}, m_k = m}), \forall m \in \{1, \dots, M\}$ ▷ Algorithm 2

(ii) *generative knowledge aggregation*

for each round $t = 1, 2, \dots, T_{KA}$ **do**

The server broadcasts w_g to clients.

for each client $k \in \mathcal{C}$ in parallel **do**

Initialize local parameters $w_k \leftarrow w_g$

for each local epoch $t = 1, \dots, T_g$ **do**

$\{(x_i, y_i)\}_{i=1}^B \sim \mathcal{D}_k$

$\{x_i\}_{i=1}^B \leftarrow \{F(x_i)\}_{i=1}^B$

$w_k \leftarrow w_k - \beta \nabla_{w_k} J_G(w_k)$

$w_g \leftarrow \text{Agg}(\{w_k\}_{k \in \mathcal{C}})$

(iii) *target network training*

for each round $t = 1, 2, \dots, T_{TN}$ **do**

The server multicasts $\{\theta_{g,m}^h\}_{m=1}^M$ to clients.

for each client $k \in \mathcal{C}$ in parallel **do**

Initialize local parameters $\theta_{k,m}^h \leftarrow \theta_{g,m}^h$

for each local epoch $t = 1, \dots, T_s$ **do**

$\{(x_i^{\text{feat}}, y_i)\}_{i=1}^B \sim G(z_i|y_i, w_g)$ ▷ synthetic feature

where $z_i \sim \mathcal{N}(\mathbf{0}, \mathbf{I})$, $y_i \sim p(y)$

$\theta_{k,m}^h \leftarrow \theta_{k,m}^h - \alpha \nabla_{\theta_{k,m}^h} J(\theta_{k,m}^h)$

for each local epoch $t = 1, \dots, T_r$ **do**

$\{(x_i^{\text{real}}, y_i)\}_{i=1}^B \sim \mathcal{D}_k$

$\theta_{k,m}^h \leftarrow \theta_{k,m}^h - \alpha \nabla_{\theta_{k,m}^h} J(\theta_{k,m}^h)$ ▷ real sample

$\theta_{g,m}^h \leftarrow \text{Agg}(\{\theta_{k,m,k}^h\}_{k \in \mathcal{C}, m_k = m}), \forall m \in \{1, \dots, M\}$

ing of a common feature extractor and a unique heterogeneous header. The parameters are denoted as $\theta_m = \{\theta^f, \theta_m^h\}$, where θ^f and θ_m^h are the parameters of common feature extractor and heterogeneous header of m -th candidate target network, respectively.

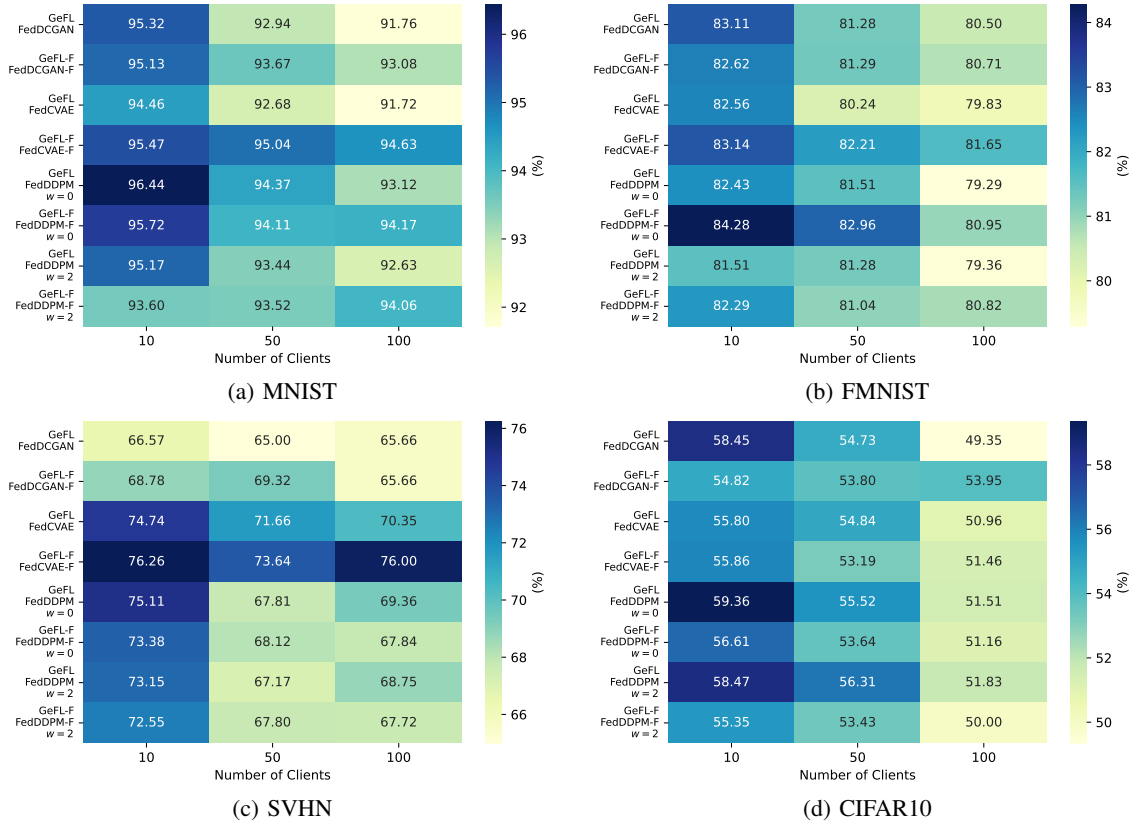


Fig. 4: Scalability in client numbers of GEFL and GEFL-F. GEFL-F exhibits less performance degradation in a large number of clients compared to GEFL.

Several FL studies have explored the use of common feature extractors [26], [32], [34], [63], [64]. They facilitate learning of global knowledge while sharing only a limited number of parameters. Our framework aligns with these practices and extends them by incorporating the use of feature-generative models. The feature-generative models learn from the feature representations (extracted by shared feature extractors), thereby capturing the collective knowledge distributed across all participating clients.

Specifically in Algorithm 3, GEFL-F is structured into four main stages: (i) *warming-up phase* for training the common feature extractor F , (ii) *generative knowledge aggregation* by training feature-generative model G_F using the warmed-up F , (iii) *target network training* on synthetic features with global knowledge from G_F , and (iv) *target network refinement* using real data. Here, J represents the cross entropy loss function, and J_G corresponds to the loss function associated with the respective generative models. The learning rates are α for the generative model G and β for the target networks.

During the warming-up phase, common feature extractors are aggregated across all clients, while heterogeneous headers are aggregated only across the clients with the same architecture. In the generative knowledge aggregation stage, feature-generative models are trained to capture the representation of intermediate features obtained by forwarding real samples through the trained common feature extractor. Then, during target network training and refinement, headers of target networks are updated by forwarding synthetic features and real

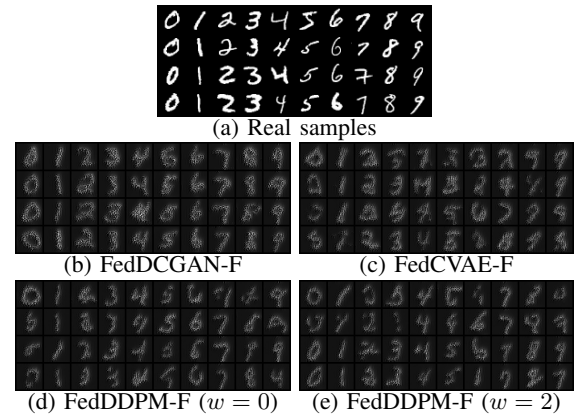


Fig. 5: Reconstructed samples generated by feature-generative models by model-inversion

samples separately.

B. Evaluation

a) *Experimental settings*: Our evaluation of GEFL-F was conducted on MNIST [38], FMNIST [39], SVHN [65] and CIFAR10 [66] datasets. We employed 10 different CNNs as our target networks, each consisting of a common feature extractor and heterogeneous header. The feature extractor is designed with a single convolutional layer followed by batch normalization and pooling layers, while the headers are 10 distinct CNNs except the feature extractor component. This results in features with a lower dimensionality. Consequently,

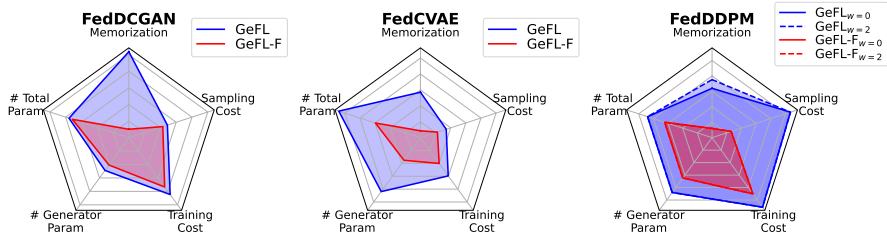


Fig. 6: **Comparison of privacy, communication and computational costs** in GEFL and GEFL-F. Lower values indicate better conditions for each component. Exact values are provided in Table III, Table V, and Table VI.

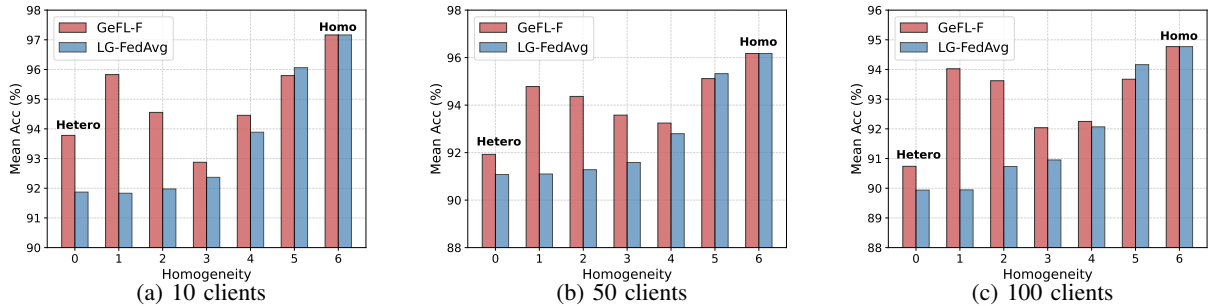


Fig. 7: **Mean classification accuracy of GEFL-F depending on the homogeneity** of model architectures on MNIST dataset. GEFL-F shows the same trend across the homogeneity regardless of the number of clients.

the reduced size of features leads to a reduction in the size of feature-generative models.

The communication rounds for warming up the feature extractor (T_{FE}) are set to 20 for MNIST and FMNIST, and 50 for SVHN and CIFAR10 to address their increased complexity. The feature-generative model is trained for $T_{KA} = 100$ rounds across MNIST, FMNIST, and SVHN and 200 for CIFAR10. Target networks are trained for $T_{TN} = 50$ rounds for MNIST, FMNIST, and SVHN, while $T_{TN} = 100$ rounds are used for CIFAR10. Additional experimental details are provided in the Appendix [1].

b) Performance, scalability, and privacy: Figure 4 illustrates the scalability performance of GEFL and GEFL-F. GEFL-F exhibits enhanced robustness compared to GEFL, effectively alleviating the performance degradation typically associated with larger client numbers. Among the generative models, GEFL-F with FedCVAE demonstrates superior effectiveness, particularly due to the reduced impact of image blurriness—an inherent limitation of VAE—when generating small-resolution features. However, for the CIFAR10 dataset, GEFL-F does not perform as effectively as it does for other datasets. This can be attributed to the lower performance of the feature extractor and target networks on CIFAR10. The degraded feature outputs from the feature extractor result in feature-generative models aggregating less effective global knowledge, which ultimately hinders the training of target networks. These observations highlight the critical role of both feature extractor quality and dataset characteristics in determining the efficacy of GEFL-F.

Furthermore, GEFL-F alleviates the privacy problem by sharing only the feature extractor and feature-generative model with the server. We measured MND in our framework, GEFL and GEFL-F, in terms of *memorization* to address the privacy.

| | FedDCGAN-F | FedCVAE-F | FedDDPM-F |
|----------------------|------------|-----------|--|
| # Total Params. | 5.191M | 5.543M | 4.428M |
| # Generator Params | 2.554M | 2.754M | 4.428M |
| Training Cost (MACs) | 159.98M | 31.88M | 503.16M |
| Sampling Cost (MACs) | 142.25M | 25.428M | 20.124G |
| MND ratio | 0.101 | 0.108 | 0.118 ($w = 0$) 0.120 ($w = 2$) |

TABLE VI: Comparison of generative models in GEFL-F

While privacy leakage is solely due to the memorization of shared generative models in GEFL, where the target networks are not shared, in GEFL-F, a common feature extractor and feature-generative model are shared between the server and clients in the FL pipeline. A promising way that attacker can take using trained feature extractor and feature-generative model is to generate synthetic features from generative model and apply model inversion using feature extractor.

We evaluated the vulnerability of GEFL-F in such scenario given a white-box feature extractor. We reconstructed the images from generated features by model inversion [51], [60]. The reconstructed images on MNIST are presented in Figure 5. Subsequently, we compare the original real images with the reconstructed ones by measuring the MND ratio, as we did in GEFL. Referring to MND ratio in Table VI and Table III, it is observed that incorporating feature-generative models mitigates privacy preservation compared to GEFL, even though it shares a common feature extractor⁷. Figure 6 illustrates that incorporating feature-generative models in GEFL-F led to reduced memorization (i.e., improved privacy preservation)

⁷While exploring novel privacy attack methods [67] and corresponding defense methods strategies, such as those involving differential privacy [68], [69] could be considered to further improve the privacy, it falls outside the scope of our current paper.

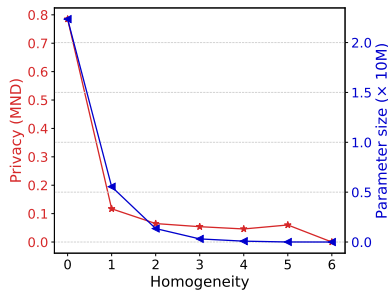


Fig. 8: **Privacy and the number of parameters of generative model of GEFL-F** across the homogeneity level of model architectures on MNIST dataset

and decreased costs such as reduced number of parameters, training cost and sampling cost compared to GEFL.

c) Trade-off across homogeneity levels: We assessed the performance of GEFL-F (FedCVAE-F) by varying the feature extractor size and the dimensionality of the generated features, transitioning from heterogeneous to homogeneous models. In Figure 7, homogeneity level (HL) 0 corresponds to GEFL, where all client models differ in architecture, while HL 6 represents complete homogeneity, with all models sharing the same architecture. As the homogeneity level increases, the dimensionality of the generator’s output decreases. The resolution of generated features for each HL is detailed in Table XI. At HL 0, no common feature extractor exists, and only model headers are trained. In contrast, at HL 6, the feature extractor serves as the entire model, requiring only the feature extractor to be trained.

In Figure 7a, while the absolute accuracy of LG-FedAvg increased due to the larger shared feature extractor among clients, GEFL-F exhibited performance gains under highly heterogeneous settings (HL 0-4) due to the augmented generated features used in training. To elaborate further on GEFL-F performance, HL 1 exhibited superior performance compared to HL 0, followed by a gradual decline until HL 3, and a subsequent increase up to HL 6. (i) GeFL exhibits gains on high levels of model heterogeneity (HL 0), but large output dimension of the generator is needed. (ii) Lowering level of heterogeneity to HL 1 enables more well-trained generator, providing both a reduced output dimension and considerably high-quality synthetic samples. (iii) However, HL 2 and 3 suffer from reduced feature diversity in synthetic samples due to its excessively low dimension. It leads to performance degradation due to insufficient information being shared among the clients. (iv) Increasing homogeneity to HL 6 expands the size of shared feature extractor, enhancing knowledge collection by sharing model parameters.

We also present the results of GEFL-F across various HMs and client numbers on MNIST, depicted in Figure 7. GEFL-F showed the performance gain and has the same trend regardless of the number of clients. Notably, GEFL-F consistently achieves the highest performance gain at a homogeneity level of 1 compared to the baseline.

Additionally, Figure 8 demonstrates that GEFL-F provides increased privacy benefits and reduced generative model parameter size as the homogeneity increases (i.e., as the common

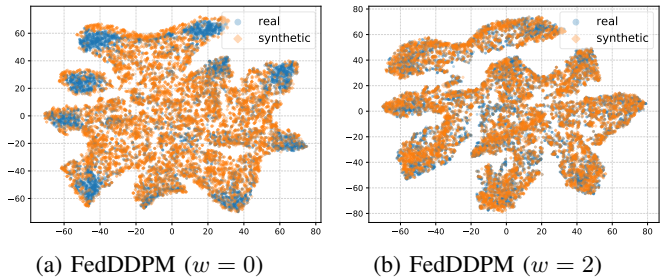


Fig. 9: **t-SNE visualization of learned representation of CIFAR10 synthetic images** generated by FedDDPM with guidance scores $w = 0$ and $w = 2$

| Dataset | Train | Update | Freeze |
|---------|----------|-------------------------|------------------|
| MNIST | Syn | 83.49 \pm 0.38 | 81.70 \pm 3.79 |
| | Real+Syn | 95.32 \pm 0.15 | 94.98 \pm 0.13 |
| FMNIST | Syn | 81.83 \pm 0.47 | 68.27 \pm 7.11 |
| | Real+Syn | 83.18 \pm 0.54 | 81.16 \pm 0.13 |

TABLE VII: **Comparison between two settings of updating FedDCGAN** when training target networks on synthetic samples (Syn) and through GEFL (Real+Syn): (i) updating GAN during target network training, and (ii) freezing it after the knowledge aggregation stage

feature extractor gets larger). This privacy enhancement aligns with the finding that features passing through a larger feature extractor contain less information about the original samples [51], [62].

V. INSIGHTS AND FINDINGS

A. Guidance of diffusion model and performance

Recent studies suggest that a lower guidance score in diffusion models often enhances downstream task performance by improving sample diversity, albeit at the expense of reduced sample quality. In Table II, our experiments on MNIST, FMNIST and CIFAR10 exhibited the consistent results where GEFL with DDPM of lower guidance score outperforms GEFL with DDPM of higher guidance score. DDPM with low guidance ($w = 0$) does not achieve considerable image quality, despite demonstrating better sample diversity [70]. We also provide t-SNE visualization results in Figure 9. We used pre-trained ResNet18 for CIFAR10 to see the ability of well-trained model learning features from real and synthetic images. The orange dots represent synthetic samples while blue dots represent real samples. The results demonstrate that synthetic samples of lower guidance score are more diverse than samples of higher guidance score. Compared to the samples of lower guidance score, the samples of higher guidance score are concentrated near the real samples..

B. Effects of GAN update

We investigated two settings for training and sampling from FedDCGAN in GEFL: (i) *freezing the FedDCGAN* after

training it for $2T$ communication rounds and (ii) *updating the FedDCGAN* for T rounds during target network training following global knowledge aggregation for T rounds. Table VII demonstrates the effect of updating FedDCGAN during target network training. The table presents results for two scenarios: training exclusively on synthetic data (Syn) and training through GEFL, which involves training target networks on both real and synthetic data (Real+Syn). Overall, updating FedDCGAN during the training of target networks achieved better performance for both datasets. This improvement is attributed to the diverse sampling from various stages of the FedDCGAN, resulting in increased mode coverage and enhanced downstream performance.

C. Evaluation of synthetic data

In this section, we highlight the differences between Syn and Real+Syn. Referring to the Table VII, in the Syn setting, compared to the Real+Syn setting, a high standard deviation of accuracies across different runs as well as degraded performance is observed. It demonstrates the effectiveness of synthetic data combined with the real data. Our proposed method, GEFL, employs both real and synthetic data and consistently showed the superior performance as well as a small standard deviation compared to the Syn, regardless of FedDCGAN freezing or updating.

Recent advances in text-to-image models and diffusion models have sparked interest in evaluating generative models based on downstream task performance, particularly when generated samples are used exclusively for training or as part of data augmentation [71], [72]. A primary work [46] proposed relevant metrics, such as classification accuracy score (CAS) and naïve augmentation score (NAS), where CAS measures the performance of target networks trained solely on synthetic data, while NAS assess the performance of target networks trained using a combination of synthetic and real data. A related area of research known as generative data augmentation (GDA) focuses on effectively leveraging synthetic datasets for augmentation alongside real data [73], [74].

In the same context, we assessed the performance of training target networks in Syn and Real+Syn (GeFL) settings within a model-heterogeneous FL setup, as presented in Table VIII. Within the GeFL framework, leveraging datasets generated by federated generative models for augmentation yielded superior performance compared to using them exclusively for training.

D. Dataset scale in GEFL

In Figure 10, we present the GEFL performance depending on dataset scales, where x-axis denotes the fraction of real dataset used. For example, MNIST has 60000 training samples and fraction rate of 0.1 employs 6000 samples in total. The real dataset is distributed over 10 clients where each client has 600 samples for the fraction rate of 0.1. Compared to FedAvg, gains of GeFL increases as the quantity of real data (possessed by whole clients) decreases. This definitely shows the effectiveness of GEFL in data-limited scenarios.

Additionally, our findings suggest that simply adding more synthetic data does not always lead to improved performance.

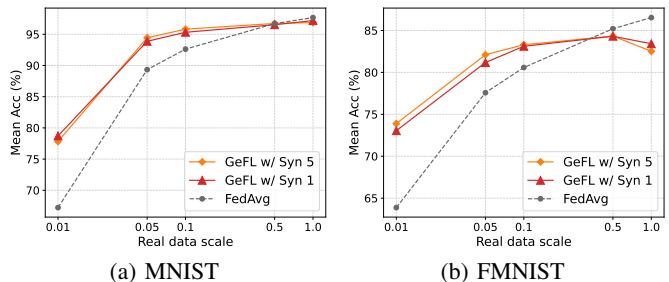


Fig. 10: Performance of GEFL with FedDCGAN across varying dataset scales demonstrates its effectiveness in scenarios where the amount of real dataset is extremely limited.

| Dataset | Train | FedDCGAN | FedCVAE | FedDDPM $w=0$ | FedDDPM $w=2$ |
|---------|----------|----------|---------|------------------|------------------|
| MNIST | Syn | 85.18 | 91.13 | 91.76 | 92.56 |
| | Real+Syn | 95.32 | 94.46 | 96.44 | 95.17 |
| FMNIST | Syn | 81.83 | 47.96 | 31.08 | 17.20 |
| | Real+Syn | 83.11 | 82.33 | 82.43 | 81.51 |

TABLE VIII: Effectiveness of generated samples from federated generative models in GEFL

The orange lines with circle markers denote the results of GeFL that generates 320 synthetic data samples ($T_s = 5$) every round, while the red lines with triangle markers denote the results of GeFL that generates 64 synthetic data samples ($T_s = 1$) every round. Notably, across different scales of real data, a fivefold increase in the quantity of synthetic samples showed the comparable performance to generating only onefold.

VI. CONCLUSION

In this paper, we proposed GEFL, a straightforward yet effective framework designed to address the challenges of model heterogeneity in FL. Our approach leverages federated generative models to efficiently aggregate knowledge from heterogeneous clients, achieving superior performance compared to baseline methods. To further enhance scalability, reduce communication and computation costs, and address privacy concerns, we introduced GEFL-F, an extension utilizing feature-generative models trained on lower-resolution features. Experimental results demonstrated the advantages of GEFL-F, including improved robustness to increasing client numbers, a significant reduction in parameters and sampling costs, and enhanced privacy preservation.

REFERENCES

- [1] H. Kang and S. Cha. [Online]. Available: <https://honggkang.github.io/gefl>
- [2] B. McMahan, E. Moore, D. Ramage, S. Hampson, and B. A. y. Arcas, "Communication-efficient learning of deep networks from decentralized data," in *International Conference on Artificial Intelligence and Statistics (AISTATS)*, 2017.
- [3] H. Kang, S. Cha, J. Shin, J. Lee, and J. Kang, "NeFL: Nested federated learning for heterogeneous clients," *arXiv preprint arXiv:2308.07761*, 2023.
- [4] A. Afonin and S. P. Karimireddy, "Towards model agnostic federated learning using knowledge distillation," in *International Conference on Learning Representations (ICLR)*, 2022.
- [5] Gemini Team, "Gemini: A family of highly capable multimodal models," *arXiv preprint arXiv:2312.11805*, 2023.

- [6] T. Brown, B. Mann, N. Ryder, M. Subbiah, J. D. Kaplan, P. Dhariwal, A. Neelakantan, P. Shyam, G. Sastry, A. Askell, A. Agarwal, A. Herbert-Voss, G. Krueger, T. Henighan, R. Child, A. Ramesh, D. Ziegler, J. Wu, C. Winter, C. Hesse, M. Chen, E. Sigler, M. Litwin, S. Gray, B. Chess, J. Clark, C. Berner, S. McCandlish, A. Radford, I. Sutskever, and D. Amodei, "Language models are few-shot learners," in *Advances in Neural Information Processing Systems (NeurIPS)*, 2020.
- [7] P. Villalobos, J. Sevilla, T. Besiroglu, L. Heim, A. Ho, and M. Hobbhahn, "Machine learning model sizes and the parameter gap," *arXiv preprint arXiv:2207.02852*, 2022.
- [8] K. Pfeiffer, M. Rapp, R. Khalili, and J. Henkel, "Federated learning for computationally constrained heterogeneous devices: A survey," *ACM Computing Surveys*, vol. 55, no. 14s, p. 1–27, Jul 2023.
- [9] T. Li, A. K. Sahu, M. Zaheer, M. Sanjabi, A. Talwalkar, and V. Smith, "Federated optimization in heterogeneous networks," in *Machine Learning and Systems (MLSys)*, 2020.
- [10] S. Horváth, S. Laskaridis, M. Almeida, I. Leontiadis, S. Venieris, and N. Lane, "FJORD: Fair and accurate federated learning under heterogeneous targets with ordered dropout," in *Advances in Neural Information Processing Systems (NeurIPS)*, 2021.
- [11] M. Kim, S. Yu, S. Kim, and S.-M. Moon, "DepthFL: Depthwise federated learning for heterogeneous clients," in *International Conference on Learning Representations (ICLR)*, 2023.
- [12] T. Lin, L. Kong, S. U. Stich, and M. Jaggi, "Ensemble distillation for robust model fusion in federated learning," in *Advances in Neural Information Processing Systems (NeurIPS)*, 2020.
- [13] W. Huang, M. Ye, and B. Du, "Learn from others and be yourself in heterogeneous federated learning," in *IEEE/CVF Conference on Computer Vision and Pattern Recognition (CVPR)*, 2022.
- [14] D. Li and J. Wang, "Fedmd: Heterogeneous federated learning via model distillation," *arXiv preprint arXiv:1910.03581*, 2019.
- [15] L. Yi, G. Wang, X. Liu, Z. Shi, and H. Yu, "FedGH: Heterogeneous federated learning with generalized global header," *arXiv preprint arXiv:2303.13137*, 2023.
- [16] H. Shin, J. K. Lee, J. Kim, and J. Kim, "Continual learning with deep generative replay," in *Advances in Neural Information Processing Systems (NeurIPS)*, 2017.
- [17] I. J. Goodfellow, J. Pouget-Abadie, M. Mirza, B. Xu, D. Warde-Farley, S. Ozair, A. Courville, and Y. Bengio, "Generative adversarial networks," in *Advances in Neural Information Processing Systems (NeurIPS)*, 2014.
- [18] D. P. Kingma and M. Welling, "Auto-encoding variational bayes," *arXiv preprint arXiv:1312.6114*, 2022.
- [19] J. Sohl-Dickstein, E. Weiss, N. Maheswaranathan, and S. Ganguli, "Deep unsupervised learning using nonequilibrium thermodynamics," in *International Conference on Machine Learning (ICML)*, 2015.
- [20] S. P. Karimireddy, S. Kale, M. Mohri, S. Reddi, S. Stich, and A. T. Suresh, "Scaffold: Stochastic controlled averaging for federated learning," in *International Conference on Machine Learning (ICML)*, 2020.
- [21] G. Hinton, O. Vinyals, and J. Dean, "Distilling the knowledge in a neural network," *arXiv preprint arXiv:1503.02531*, 2015.
- [22] H. Seo, J. Park, S. Oh, M. Bennis, and S.-L. Kim, "Federated knowledge distillation," *arXiv preprint arXiv:2011.02367*, 2020.
- [23] C. Wu, F. Wu, L. Lyu, Y. Huang, and X. Xie, "Communication-efficient federated learning via knowledge distillation," *Nature Communications*, vol. 13, no. 1, Apr. 2022.
- [24] X. Li, B. Chen, and W. Lu, "FedDKD: Federated learning with decentralized knowledge distillation," *Applied Intelligence*, vol. 53, no. 15, p. 18547–18563, Feb. 2023.
- [25] E. Diao, J. Ding, and V. Tarokh, "HeteroFL: Computation and communication efficient federated learning for heterogeneous clients," in *International Conference on Learning Representations (ICLR)*, 2021.
- [26] P. P. Liang, T. Liu, L. Ziyin, R. Salakhutdinov, and L.-P. Morency, "Think locally, act globally: Federated learning with local and global representations," *arXiv preprint arXiv:2001.01523*, 2020.
- [27] T. Shen, J. Zhang, X. Jia, F. Zhang, G. Huang, P. Zhou, K. Kuang, F. Wu, and C. Wu, "Federated mutual learning," *arXiv preprint arXiv:2006.16765*, 2020.
- [28] J. Wang, X. Yang, S. Cui, L. Che, L. Lyu, D. Xu, and F. Ma, "Towards personalized federated learning via heterogeneous model reassembly," *arXiv preprint arXiv:2308.08643*, 2023.
- [29] H. Wen, Y. Wu, J. Li, and H. Duan, "Communication-efficient federated data augmentation on non-iid data," in *IEEE/CVF Conference on Computer Vision and Pattern Recognition Workshops (CVPRW)*, 2022.
- [30] E. Jeong, S. Oh, H. Kim, J. Park, M. Bennis, and S.-L. Kim, "Communication-efficient on-device machine learning: Federated distillation and augmentation under non-iid private data," *arXiv preprint arXiv:1811.11479*, 2023.
- [31] M. Rasouli, T. Sun, and R. Rajagopal, "FedGAN: Federated generative adversarial networks for distributed data," *arXiv preprint arXiv:2006.07228*, 2020.
- [32] Z. Zhu, J. Hong, and J. Zhou, "Data-free knowledge distillation for heterogeneous federated learning," in *International Conference on Machine Learning (ICML)*, 2021.
- [33] L. Zhang, L. Shen, L. Ding, D. Tao, and L. Duan, "Fine-tuning global model via data-free knowledge distillation for non-iid federated learning," in *IEEE/CVF Conference on Computer Vision and Pattern Recognition (CVPR)*, 2022.
- [34] Y. Wu, Y. Kang, J. Luo, Y. He, and Q. Yang, "FedCG: Leverage conditional gan for protecting privacy and maintaining competitive performance in federated learning," *arXiv preprint arXiv:2111.08211*, 2021.
- [35] K. He, X. Zhang, S. Ren, and J. Sun, "Deep residual learning for image recognition," in *IEEE/CVF Conference on Computer Vision and Pattern Recognition (CVPR)*, 2016.
- [36] M. Tan and Q. Le, "EfficientNet: Rethinking model scaling for convolutional neural networks," in *International Conference on Machine Learning (ICML)*. PMLR, 2019, pp. 6105–6114.
- [37] A. G. Howard, M. Zhu, B. Chen, D. Kalenichenko, W. Wang, T. Weyand, M. Andreetto, and H. Adam, "Mobilenets: Efficient convolutional neural networks for mobile vision applications," *arXiv preprint arXiv:1704.04861*, 2017.
- [38] Y. LeCun, L. Bottou, Y. Bengio, and P. Haffner, "Gradient-based learning applied to document recognition," *Proceedings of the IEEE*, vol. 86, no. 11, pp. 2278–2324, 1998.
- [39] H. Xiao, K. Rasul, and R. Vollgraf, "Fashion-mnist: a novel image dataset for benchmarking machine learning algorithms," *arXiv preprint arXiv:1708.07747*, 2017.
- [40] A. Krizhevsky *et al.*, "Learning multiple layers of features from tiny images," *Master's thesis, Department of Computer Science, University of Toronto*, 2009.
- [41] A. Radford, L. Metz, and S. Chintala, "Unsupervised representation learning with deep convolutional generative adversarial networks," in *International Conference on Learning Representations (ICLR)*, 2016.
- [42] Y. Pu, Z. Gan, R. Henao, X. Yuan, C. Li, A. Stevens, and L. Carin, "Variational autoencoder for deep learning of images, labels and captions," in *Advances in Neural Information Processing Systems (NeurIPS)*, 2016.
- [43] J. Ho, A. Jain, and P. Abbeel, "Denoising diffusion probabilistic models," in *Advances in Neural Information Processing Systems (NeurIPS)*, 2020.
- [44] J. Ho and T. Salimans, "Classifier-free diffusion guidance," in *NeurIPS 2021 Workshop on Deep Generative Models and Downstream Applications*, 2021.
- [45] M. Heusel, H. Ramsauer, T. Unterthiner, B. Nessler, and S. Hochreiter, "Gans trained by a two time-scale update rule converge to a local nash equilibrium," in *Advances in Neural Information Processing Systems (NeurIPS)*, 2017.
- [46] S. Ravuri and O. Vinyals, "Classification accuracy score for conditional generative models," in *Advances in Neural Information Processing Systems (NeurIPS)*, 2019.
- [47] H. Zhang, M. Cisse, Y. N. Dauphin, and D. Lopez-Paz, "mixup: Beyond empirical risk minimization," in *International Conference on Learning Representations (ICLR)*, 2018.
- [48] S. Yun, D. Han, S. J. Oh, S. Chun, J. Choe, and Y. Yoo, "Cutmix: Regularization strategy to train strong classifiers with localizable features," in *IEEE/CVF Conference on Computer Vision and Pattern Recognition (CVPR)*, 2019.
- [49] D. Hendrycks, N. Mu, E. D. Cubuk, B. Zoph, J. Gilmer, and B. Lakshminarayanan, "Augmix: A simple data processing method to improve robustness and uncertainty," in *International Conference on Learning Representations (ICLR)*, 2019.
- [50] E. D. Cubuk, B. Zoph, D. Mane, V. Vasudevan, and Q. V. Le, "Autoaugment: Learning augmentation policies from data," *arXiv preprint arXiv:1805.09501*, 2018.
- [51] M. D. Zeiler and R. Fergus, "Visualizing and understanding convolutional networks," in *European Conference on Computer Vision (ECCV)*, 2014.
- [52] J. Geiping, H. Bauermeister, H. Dröge, and M. Moeller, "Inverting gradients-how easy is it to break privacy in federated learning?" *Advances in Neural Information Processing Systems (NeurIPS)*, 2020.
- [53] G. van den Burg and C. Williams, "On memorization in probabilistic deep generative models," in *Advances in Neural Information Processing Systems (NeurIPS)*, 2021.
- [54] G. Somepalli, V. Singla, M. Goldblum, J. Geiping, and T. Goldstein, "Diffusion art or digital forgery? investigating data replication in diffu-

- sion models,” in *IEEE/CVF Conference on Computer Vision and Pattern Recognition (CVPR)*, 2023.
- [55] R. Webster, J. Rabin, L. Simon, and F. Jurie, “Detecting overfitting of deep generative networks via latent recovery,” in *IEEE/CVF Conference on Computer Vision and Pattern Recognition (CVPR)*, 2019.
- [56] X. Sun, N. Gazagnadou, V. Sharma, L. Lyu, H. Li, and L. Zheng, “Privacy assessment on reconstructed images: Are existing evaluation metrics faithful to human perception?” in *Advances in Neural Information Processing Systems (NeurIPS)*, 2023.
- [57] R. Zhang, P. Isola, A. A. Efros, E. Shechtman, and O. Wang, “The unreasonable effectiveness of deep features as a perceptual metric,” in *IEEE/CVF Conference on Computer Vision and Pattern Recognition (CVPR)*, 2018.
- [58] Y. Zhao, M. Li, L. Lai, N. Suda, D. Civin, and V. Chandra, “Federated learning with non-iid data,” *arXiv preprint arXiv:1806.00582*, 2018.
- [59] A. Mahendran and A. Vedaldi, “Understanding deep image representations by inverting them,” in *IEEE/CVF Conference on Computer Vision and Pattern Recognition (CVPR)*, 2015.
- [60] A. Dosovitskiy and T. Brox, “Inverting visual representations with convolutional networks,” in *IEEE/CVF Conference on Computer Vision and Pattern Recognition (CVPR)*, 2016.
- [61] A. Brock, J. Donahue, and K. Simonyan, “Large scale GAN training for high fidelity natural image synthesis,” *arXiv preprint arXiv:1809.11096*, 2018.
- [62] L. A. Gatys, A. S. Ecker, and M. Bethge, “Image style transfer using convolutional neural networks,” in *IEEE/CVF Conference on Computer Vision and Pattern Recognition (CVPR)*, 2016.
- [63] J. Jang, H. Ha, D. Jung, and S. Yoon, “Fedclassavg: Local representation learning for personalized federated learning on heterogeneous neural networks,” in *Proceedings of the 51st International Conference on Parallel Processing*, 2022, pp. 1–10.
- [64] J. Mori, I. Teranishi, and R. Furukawa, “Continual horizontal federated learning for heterogeneous data,” in *2022 International Joint Conference on Neural Networks (IJCNN)*. IEEE, 2022, pp. 1–8.
- [65] Y. Netzer, T. Wang, A. Coates, A. Bissacco, B. Wu, and A. Y. Ng, “Reading digits in natural images with unsupervised feature learning,” in *NIPS Workshop on Deep Learning and Unsupervised Feature Learning*, 2011.
- [66] A. Krizhevsky, V. Nair, and G. Hinton, “CIFAR-10 (Canadian Institute for Advanced Research),” <http://www.cs.toronto.edu/~kriz/cifar.html>.
- [67] J. Jeon, K. Lee, S. Oh, J. Ok *et al.*, “Gradient inversion with generative image prior,” *Advances in Neural Information Processing Systems (NeurIPS)*, vol. 34, pp. 29 898–29 908, 2021.
- [68] M. Abadi, A. Chu, I. Goodfellow, H. B. McMahan, I. Mironov, K. Talwar, and L. Zhang, “Deep learning with differential privacy,” in *Proceedings of the 2016 ACM SIGSAC conference on computer and communications security*, 2016, pp. 308–318.
- [69] L. Xie, K. Lin, S. Wang, F. Wang, and J. Zhou, “Differentially private generative adversarial network,” *arXiv preprint arXiv:1802.06739*, 2018.
- [70] L. Fan, K. Chen, D. Krishnan, D. Katabi, P. Isola, and Y. Tian, “Scaling laws of synthetic images for model training... for now,” *arXiv preprint arXiv:2312.04567*, 2023.
- [71] Y. Tian, L. Fan, P. Isola, H. Chang, and D. Krishnan, “Stablerep: Synthetic images from text-to-image models make strong visual representation learners,” in *Advances in Neural Information Processing Systems (NeurIPS)*, 2023.
- [72] S. Azizi, S. Kornblith, C. Saharia, M. Norouzi, and D. J. Fleet, “Synthetic data from diffusion models improves imagenet classification,” *Transactions on Machine Learning Research*, 2023.
- [73] K. Shmelkov, C. Schmid, and K. Alahari, “How good is my GAN?” in *Proceedings of the European conference on computer vision (ECCV)*, 2018, pp. 213–229.
- [74] S. Yamaguchi, D. Chijiwa, S. Kanai, A. Kumagai, and H. Kashima, “Regularizing neural networks with meta-learning generative models,” in *Thirty-seventh Conference on Neural Information Processing Systems*, 2023.
- [75] O. Ronneberger, P. Fischer, and T. Brox, “U-Net: Convolutional networks for biomedical image segmentation,” in *International Conference on Medical Image Computing and Computer-Assisted Intervention*, 2015.
- [76] T. Pearce, H. H. Tan, M. Zeraatkar, and X. Zhao, “Github.” [Online]. Available: https://github.com/TeaPearce/Conditional_Diffusion_MNIST
- [77] S. Ioffe and C. Szegedy, “Batch normalization: accelerating deep network training by reducing internal covariate shift,” in *International Conference on Machine Learning (ICML)*, 2015.
- [78] A. F. Agarap, “Deep learning using rectified linear units (relu),” *arXiv preprint arXiv:1803.08375*, 2018.

- [79] C. Meehan, K. Chaudhuri, and S. Dasgupta, “A non-parametric test to detect data-copying in generative models,” in *International Conference on Artificial Intelligence and Statistics (AISTATS)*, 2020.



Honggu Kang received the B.Sc. degree (*summa cum laude*) in electronic engineering from Hanyang University, Seoul, South Korea, in 2017, and the M.Sc. and Ph.D. degrees from the School of Electrical Engineering, Korea Advanced Institute of Science and Technology (KAIST), Daejeon, South Korea, in 2019 and 2024, respectively.

He is currently a staff engineer in Samsung Electronics, Suwon, South Korea since 2024. His research interests include edge AI, federated learning, signal processing for wireless communications, and unmanned aerial vehicle communications. He was a recipient of the Korean Institute of Communications and Information Sciences (KICS) Fall Symposium Best Paper Award, in 2019.



Seohyeon Cha received the B.S. (*summa cum laude*) and M.S. degrees from the School of Electrical Engineering, Korea Advanced Institute of Science and Technology (KAIST), Daejeon, South Korea, in 2022 and 2024, respectively.

She is currently pursuing the Ph.D. degree in Electrical and Computer Engineering with The University of Texas at Austin, Austin, TX, USA. Her primary research interests include collaborative learning systems, federated learning, and trustworthy machine learning. She was a recipient of the National Science and Engineering Scholarship.



Joonhyuk Kang received the B.S.E. and M.S.E. degrees from Seoul National University, Seoul, South Korea, in 1991 and 1993, respectively, and the Ph.D. degree in electrical and computer engineering from The University of Texas at Austin, Austin, in 2002. From 1993 to 1998, he was a Research Staff Member at Samsung Electronics, Suwon, South Korea, where he was involved in the development of DSP-based real-time control systems. In 2000, he was with Cwill Telecommunications, Austin, TX, USA, where he participated in the project for multicarrier CDMA systems with antenna array. He was a Visiting Scholar with the School of Engineering and Applied Sciences, Harvard University, Cambridge, MA, USA, from 2008 to 2009. He served as Head of the School of Electrical Engineering (EE), KAIST, Daejeon, South Korea. His research interests include signal processing and machine learning for wireless communication systems. He is a life-member of the Korea Information and Communication Society and the Tau Beta Pi (the Engineering Honor Society). He was a recipient of IEEE VTS Jack Neubauer Memorial Award in 2021 for his paper titled “Mobile Edge Computing via a UAV-Mounted Cloudlet: Optimization of Bit Allocation and Path Planning.”

APPENDIX A
EXPERIMENTAL DETAILS

All hyperparameter settings for GEFL and GEFL-F are summarized in Table IX and Table X. Table IX outlines the hyperparameter configurations for training target networks in GEFL and GEFL-F. Notably, T_{FE} is exclusive to training the feature extractor in GEFL-F.

Table X presents the hyperparameter settings for training federated generative models (FedGens) in GEFL and GEFL-F. The latent dimensions, denoted as d_g and d_d , correspond to parameters of FedDCGAN and FedDCGAN-F, respectively. Similarly, the latent size l is used for FedCVAE and FedCVAE-F, while n_{feat} pertains to FedDDPM and FedDDPM-F. Details on these parameters are provided in Appendix B-A.

The number of FL communication rounds for training generative models, T_{KA} , in Table X indicates the total rounds used to update the FedGens (e.g., FedDCGANs) during the training process in both GEFL and GEFL-F. For instance, under the *update* setting discussed in Section V-B, FedDCGAN is updated for half of the rounds ($T_{KA}/2$) during global knowledge aggregation stages and subsequently updated for the remaining half during target network training. Conversely, in the *freeze* setting, FedDCGAN is updated for the full T_{KA} rounds exclusively during the global knowledge aggregation stages.

The results presented in Table 8 and Table 7 were obtained based on the configurations outlined in Table XI. Detailed model architectures used to generate feature outputs are provided in Appendix B.

For baseline evaluation, we applied a proximal term with a scaling factor of 1×10^{-2} for FedProx [9]. For AvgKD [4], pseudo labels were aggregated from the outputs of 10 heterogeneous models. In the case of FedDF [12], we used SVHN as the public dataset for MNIST, and CIFAR10 as the public dataset for FMNIST. For LG-FedAvg [26], the first convolutional layer was averaged across all heterogeneous models, while subsequent layers were averaged within their respective submodels.

For evaluating baselines, we used $1e-2$ multiplied to proximal term for FedProx [9]. Pseudo labels are aggregated from the outputs of 10 heterogeneous models for AvgKD [4]. For FedDF [12], we used SVHN as the public dataset for MNIST, CIFAR10 as the public dataset for FMNIST, and CIFAR100 as the public dataset for CIFAR10. For LG-FedAvg [26] the first conv layer was employed as averaging over all the heterogeneous models while the other layers are averaged across submodels.

To evaluate the FID and IS scores, we generated 1,000 conditional images uniformly distributed across classes, with 100 images per class.

| | MNIST | FMNIST | CIFAR10 | SVHN |
|------------------------|---------|--------|---------|------|
| T_{TN} | 50 | 50 | 100 | 100 |
| Optimizer | SGD | SGD | SGD | SGD |
| Learning rate α | 1e-1 | 1e-1 | 1e-1 | 1e-1 |
| Batch size B | 64 | 64 | 128 | 64 |
| Data fraction | 0.1 | 0.1 | 0.5 | 0.1 |
| $T_w/T_g/T_s/T_r$ | 5/5/1/5 | | | |
| T_{FE} | 20 | 20 | 50 | 50 |

TABLE IX: Hyperparameters for training **target networks** in GeFL and GeFL-F and **feature extractor** in GeFL-F.

| | FedDCGAN | FedCVAE | FedDDPM | FedDCGAN-F | FedCVAE-F | FedDDPM-F | |
|-------------------------------|---------------------------------|---------------------------------|--------------------|--------------------|--------------------|--------------------|-----|
| Optimizer | Adam | Adam | Adam | Adam | Adam | Adam | |
| Learning rate β | 2×10^{-4} | 1×10^{-3} | 1×10^{-4} | 2×10^{-4} | 1×10^{-3} | 1×10^{-4} | |
| Weight decay | - | 1×10^{-3} | - | - | 1×10^{-3} | - | |
| b_1, b_2 (Adam) | 0.5, 0.999 | - | - | 0.5, 0.999 | - | - | |
| CIFAR10 | Latent dimension (d_g, d_d) | 256, 64 | - | - | 256, 64 | - | |
| | Latent size l | - | 50 | - | - | 50 | |
| | n_{feat} (of U-Net in DDPM) | - | - | 128 | - | - | 128 |
| | Time step | - | - | 400 | - | - | 500 |
| | Batch size B | 64 | 64 | 64 | 64 | 64 | 64 |
| | T_{KA} | 200 | 200 | 200 | 200 | 200 | 200 |
| | MNIST FMNIST SVHN | Latent dimension (d_g, d_d) | 128, 128 | - | - | 128, 128 | - |
| Latent size l | | - | 16 | - | - | 16 | |
| n_{feat} (of U-Net in DDPM) | | - | - | 128 | - | - | 128 |
| Time step | | - | - | 100 | - | - | 100 |
| Batch size B | | 64 | 64 | 64 | 64 | 64 | 64 |
| T_{KA} | | 100 | 100 | 100 | 100 | 100 | 100 |

TABLE X: Hyperparameters for training both **generative models and feature-generative models** in a federated scenario.

| Homogeneity level | 0 | 1 | 2 | 3 | 4 | 5 | 6 |
|-------------------|-------|-------|-----|-----|-----|-----|----|
| Channel | 1 | 3 | 10 | 20 | 40 | 80 | - |
| Image size | 32x32 | 16x16 | 8x8 | 4x4 | 2x2 | 1x1 | - |
| T_{FE} | 0 | 20 | 20 | 20 | 50 | 60 | 70 |
| T_{TN} | 70 | 50 | 50 | 50 | 20 | 10 | 0 |
| T_{KA} | 100 | 100 | 100 | 100 | 100 | 100 | - |

TABLE XI: The size of features according to the homogeneity level

APPENDIX B MODEL ARCHITECTURE

A. Generative models

1) *GAN*: GAN introduces a generator with parameters θ_g , $G(z; \theta_g)$, to learn the distribution over training data where z denotes input noise variables that are mapped to data space. A discriminator $D(x; \theta_d)$ that outputs a single scalar is also introduced. $D(x)$ represents the probability that x came from the data rather than from G . D is trained to correctly classify whether the input is from training data or samples from G . G is simultaneously trained to minimize $\log(1 - D(G(z)))$ to fake D . In other words, D and G play the following two-player minimax game: $\min_G \max_D \mathbb{E}_{x \sim p(x)} [\log D(x)] + \mathbb{E}_{z \sim p_z(z)} [\log(1 - D(G(z)))]$.

Our implementation for FedDCGAN and FedDCGAN-F consist of generator and discriminator. Referring to Table XIIa and Table XIIIa, for the generator, 100 dimensional uniform distribution latent input is projected to step 1 and 2 while conditional label is projected to step 3 and 4⁸. Two projected outputs are then concatenated and projected to following steps. Referring to Table XIIb and Table XIIIb, for the discriminator, image is projected to step 1 and label is projected to step 2. Two projected outputs are then concatenated and projected to following steps. We used $(d_g, d_d, c) = (128, 128, 1)$ for MNIST and FMNIST, $(256, 64, 3)$ for CIFAR10 and $(128, 128, 3)$ for CelebA and SVHN.

| Step | Layer | Parameters | Activation |
|------|-----------------|-------------------------|------------|
| 1 | ConvTranspose2d | $(100, 2d_g, 4, 1, 0)$ | relu |
| 2 | BatchNorm2d | $2d_g$ | |
| 3 | ConvTranspose2d | $(10, 2d_g, 4, 1, 0)$ | relu |
| 4 | BatchNorm2d | $2d_g$ | |
| 5 | Concatenate | | |
| 6 | ConvTranspose2d | $(4d_g, 2d_g, 4, 2, 1)$ | relu |
| 7 | BatchNorm2d | $2d_g$ | |
| 8 | ConvTranspose2d | $(2d_g, 2d_g, 4, 2, 1)$ | relu |
| 9 | BatchNorm2d | d_g | |
| 10 | ConvTranspose2d | $(d_g, c, 4, 2, 1)$ | tanh |

(a) FedDCGAN Generator Architecture

| Step | Layer | Parameters | Activation |
|------|-------------|-------------------------|-----------------|
| 1 | Conv2d | $(c, d_d/2, 4, 2, 1)$ | leaky-relu(0.2) |
| 2 | Conv2d | $(10, d_d/2, 4, 2, 1)$ | leaky-relu(0.2) |
| 3 | Concatenate | | |
| 4 | Conv2d | $(d_d, 2d_d, 4, 2, 1)$ | leaky-relu(0.2) |
| 5 | BatchNorm2d | $2d_d$ | |
| 6 | Conv2d | $(2d_d, 4d_d, 4, 2, 1)$ | leaky-relu(0.2) |
| 7 | BatchNorm2d | $4d_d$ | |
| 8 | Conv2d | $(4d_d, 1, 4, 1, 0)$ | sigmoid |

(b) FedDCGAN Discriminator Architecture

TABLE XII: Architectures of FedDCGAN Generator and Discriminator.

| Step | Layer | Parameters | Activation |
|------|-----------------|-------------------------|-----------------|
| 1 | ConvTranspose2d | $(100, 2d_g, 4, 1, 0)$ | leaky-relu(0.2) |
| 2 | BatchNorm2d | $2d_g$ | |
| 3 | ConvTranspose2d | $(10, 2d_g, 4, 1, 0)$ | leaky-relu(0.2) |
| 4 | BatchNorm2d | $2d_g$ | |
| 5 | Concatenate | | |
| 6 | ConvTranspose2d | $(4d_g, 2d_g, 4, 2, 1)$ | leaky-relu(0.2) |
| 7 | BatchNorm2d | $2d_g$ | |
| 8 | ConvTranspose2d | $(2d_g, c, 4, 2, 1)$ | relu |

(a) FedDCGAN-F Generator Architecture

| Step | Layer | Parameters | Activation |
|------|-------------|-------------------------|-----------------|
| 1 | Conv2d | $(c, d_d/2, 4, 2, 1)$ | leaky-relu(0.2) |
| 2 | Conv2d | $(10, d_d/2, 4, 2, 1)$ | leaky-relu(0.2) |
| 3 | Concatenate | | |
| 4 | Conv2d | $(d_d, 2d_d, 4, 2, 1)$ | leaky-relu(0.2) |
| 5 | BatchNorm2d | $2d_d$ | |
| 6 | Conv2d | $(2d_d, 4d_d, 4, 2, 1)$ | leaky-relu(0.2) |
| 7 | BatchNorm2d | $4d_d$ | |
| 8 | Conv2d | $(4d_d, 1, 2, 1, 0)$ | sigmoid |

(b) FedDCGAN-F Discriminator Architecture

TABLE XIII: Architectures of FedDCGAN-F Generator and Discriminator.

2) *VAE*: VAE is trained by maximum likelihood so that the model is likely to produce training set samples. Therefore, VAE aims to maximize the probability of each x in the training set according to $\max P(x) = \int P(x|z; \theta)P(z)dz$. VAE consists of encoding x into z and decoding z into x . The decoder maps latent variable z to data space where z is drawn from $\mathcal{N}(0, I)$. However, $P(x|z)$ is nearly zero for most z that the encoder sample z 's that are likely to have produced x . A new function $Q(z|x)$ is introduced to take a value of x and give a distribution over z 's that are likely to produce x . $\sigma\mathcal{N}(0, I) + \mu$. Then, the loss function is written as follows: $\log P(x) - \mathcal{D}[Q(z|x)||P(z|x)] = \mathbb{E}_{z \sim Q} [\log P(x|z)] - \mathcal{D}[Q(z|x)||P(z)]$, where \mathcal{D}

⁸Descriptions of ConvTranspose2d, BatchNorm2d, relu, leaky-relu, and Conv2d are based on the documentation provided by the PyTorch library (<https://pytorch.org/docs/stable/nn.html>).

denotes KL divergence. Note that in testing-time, the samples are generated by decoding by drawing z from $\mathcal{N}(0, I)$ without encoding.

Our implementation for FedCVAE and FedCVAE-F consist of encoder and decoder. Referring to Table XIVa and Table XVa, for encoder, input image and label of same size (e.g., 32×32 , 16×16) are concatenated to add a channel (step 1) and the concatenated input is projected to following steps until step 11. Then, the output is respectively projected to two different layers, $\text{Linear}(1024, l)$ (or $\text{Linear}(512, l)$) for μ and $\text{Linear}(1024, l)$ (or $\text{Linear}(512, l)$) for σ . Referring to Table XIVb and Table XVb, for decoder, z (of dimension l) and label (with dimension of number of the classes) are concatenated and projected to following steps. We used $(c, l, z) = (1, 16)$ for MNIST and FMNIST, $(3, 50)$ for CIFAR10, $(3, 32)$ for CelebA, and $(3, 16)$ for SVHN.

| Step | Layer | Parameters | Activation |
|------|------------------------|---------------------------------|------------|
| 1 | Concatenate | Input image + label (1 channel) | |
| 2 | Conv2d | $(c + 1, 64, 4, 2, 1)$ | relu |
| 3 | BatchNorm2d | 64 | |
| 4 | Conv2d | $(64, 128, 4, 2, 1)$ | relu |
| 5 | BatchNorm2d | 128 | |
| 6 | Conv2d | $(128, 256, 4, 2, 1)$ | relu |
| 7 | BatchNorm2d | 256 | |
| 8 | Conv2d | $(256, 512, 4, 2, 1)$ | relu |
| 9 | BatchNorm2d | 512 | |
| 10 | Conv2d | $(512, 1024, 4, 2, 1)$ | relu |
| 11 | BatchNorm2d | 1024 | |
| 12 | Linear (for μ) | $1024, l$ | |
| 13 | Linear (for σ) | $1024, l$ | |

(a) FedCVAE Encoder Architecture

| Step | Layer | Parameters | Activation |
|------|-----------------|------------------------|------------|
| 1 | Concatenate | $z + \text{label}$ | |
| 2 | Linear | $l + 10$ | |
| 3 | ConvTranspose2d | $(1024, 512, 4, 2, 1)$ | relu |
| 4 | BatchNorm2d | 512 | |
| 5 | ConvTranspose2d | $(512, 256, 4, 2, 1)$ | relu |
| 6 | BatchNorm2d | 256 | |
| 7 | ConvTranspose2d | $(256, 128, 4, 2, 1)$ | relu |
| 8 | BatchNorm2d | 128 | |
| 9 | ConvTranspose2d | $(128, 64, 4, 2, 1)$ | relu |
| 10 | BatchNorm2d | 64 | |
| 11 | ConvTranspose2d | $(64, c, 4, 2, 1)$ | relu |

(b) FedCVAE Decoder Architecture

TABLE XIV: Architectures of FedCVAE Encoder and Decoder.

| Step | Layer | Parameters | Activation |
|------|------------------------|---------------------------------|------------|
| 1 | Concatenate | Input image + label (1 channel) | |
| 2 | Conv2d | $(c + 1, 64, 4, 2, 1)$ | relu |
| 3 | BatchNorm2d | 64 | |
| 4 | Conv2d | $(64, 128, 4, 2, 1)$ | relu |
| 5 | BatchNorm2d | 128 | |
| 6 | Conv2d | $(128, 256, 4, 2, 1)$ | relu |
| 7 | BatchNorm2d | 256 | |
| 8 | Conv2d | $(256, 512, 4, 2, 1)$ | relu |
| 9 | BatchNorm2d | 512 | |
| 10 | Linear (for μ) | $512, l$ | |
| 11 | Linear (for σ) | $512, l$ | |

(a) FedCVAE-F Encoder Architecture

| Step | Layer | Parameters | Activation |
|------|-----------------|-----------------------|------------|
| 1 | Concatenate | $z + \text{label}$ | |
| 2 | Linear | $l + 10$ | |
| 3 | ConvTranspose2d | $(512, 256, 4, 2, 1)$ | relu |
| 4 | BatchNorm2d | 256 | |
| 5 | ConvTranspose2d | $(256, 128, 4, 2, 1)$ | relu |
| 6 | BatchNorm2d | 128 | |
| 7 | ConvTranspose2d | $(128, 64, 4, 2, 1)$ | relu |
| 8 | BatchNorm2d | 64 | |
| 9 | ConvTranspose2d | $(64, c, 4, 2, 1)$ | relu |

(b) FedCVAE-F Decoder Architecture

TABLE XV: Architectures of FedCVAE-F Encoder and Decoder.

3) *DDPM*: Diffusion models represent latent variable models of $p_\theta(\mathbf{x}_0) := \int p_\theta(\mathbf{x}_{0:T}) d\mathbf{x}_{1:T}$, where $\mathbf{x}_1, \dots, \mathbf{x}_T$ denote latent variables with the same dimensionality as the data $\mathbf{x}_0 \sim q(\mathbf{x}_0)$. The reverse process is defined as a Markov chain and the forward process or diffusion process, also follows a Markov chain introducing Gaussian noise to the data based on a variance schedule. An important property of the forward process is its capability to generate samples \mathbf{x}_t at any time step t in closed form. Training is feasible by optimizing random terms of L as: $\mathbb{E}_q[\mathcal{D}(q(\mathbf{x}_T | \mathbf{x}_0) || p(\mathbf{x}_T)) + \sum_{t>1} \mathcal{D}(q(\mathbf{x}_{t-1} | \mathbf{x}_t, \mathbf{x}_0) || p_\theta(\mathbf{x}_{t-1} | \mathbf{x}_t)) - \log p_\theta(\mathbf{x}_0 | \mathbf{x}_1)]$, where \mathcal{D} denotes KL divergence.

Our implementation of FedDDPM and FedDDPM-F are based on the backbone of a U-Net [75] and we modified it following [76] (refer to our code) [1]. We utilized FedDDPM with a time step of $T = 100$ for MNIST, FMNIST, and SVHN, and $T = 400$ for CIFAR10. Similarly, FedDDPM-F was employed with a time step of $T = 100$ for MNIST, FMNIST, and SVHN, and $T = 500$ for CIFAR10.

B. Target network architectures

For MNIST, FMNIST, SVHN, and CIFAR10 datasets, we employed 10 heterogeneous CNN architectures, detailed in Table XVI, Table XVII, and Table XVIII. In all tables, $\text{conv}(c, k, p)$ denotes a 2d convolutional layer, where c is the output channel size, k is the kernel size, and p is the padding size. $\text{bn}(c)$ represents a batch normalization layer [77] with c denoting the channel size. The term relu denotes the rectified linear layer [78], and $\text{maxpool}(k, s, p)$ denotes a max-pooling layer, where k is the kernel size, s is the stride, and p is the padding size. Finally, $\text{fc}(in/out)$ indicates a fully connected layer, where in is the number of input nodes and out is the number of output nodes.

In the experiments depicted in Figure 7, we utilized 10 CNN-10 models to ensure fair comparison. Despite utilizing equivalent models, as heterogeneity increases, the common feature extractor (θ_g^f) decreases in size. Note that θ_g^f is aggregated across the heterogeneous models. For instance, CNN-10 in Table XVI, at homogeneity level 1, θ_g^f consists of conv(3,3×3,1) followed by bn(3), relu, maxpool(2×2,2,0). On the other hand, at homogeneity level 2, conv(10,3×3,1) followed by relu, maxpool(2×2,2,0) are additionally included in θ_g^f .

| CNN-1 | CNN-2 | CNN-3 | CNN-4 | CNN-5 | CNN-6 | CNN-7 | CNN-8 | CNN-9 | CNN-10 |
|--|--|--|--|--|--|--|---|---|--|
| conv(3,3×3,1) bn(3) relu maxpool(2×2,2,0) conv(16,3×3,1) relu maxpool(2×2,2,0) | conv(3,3×3,1) bn(3) relu maxpool(2×2,2,0) conv(16,3×3,1) relu maxpool(2×2,2,0) conv(32,3×3,1) relu maxpool(2×2,2,0) | conv(3,3×3,1) bn(3) relu maxpool(2×2,2,0) conv(20,3×3,1) relu maxpool(2×2,2,0) conv(40,3×3,1) relu maxpool(2×2,2,0) | conv(3,3×3,1) bn(3) relu maxpool(2×2,2,0) conv(10,3×3,1) relu maxpool(2×2,2,0) conv(20,3×3,1) relu maxpool(2×2,2,0) | conv(3,3×3,1) bn(3) relu maxpool(2×2,2,0) conv(16,3×3,1) relu maxpool(2×2,2,0) conv(32,3×3,1) relu maxpool(2×2,2,0) conv(64,3×3,1) relu maxpool(2×2,2,0) | conv(3,3×3,1) bn(3) relu maxpool(2×2,2,0) conv(20,3×3,1) relu maxpool(2×2,2,0) conv(40,3×3,1) relu maxpool(2×2,2,0) conv(80,3×3,1) relu maxpool(2×2,2,0) | conv(3,3×3,1) bn(3) relu maxpool(2×2,2,0) conv(10,3×3,1) relu maxpool(2×2,2,0) conv(20,3×3,1) relu maxpool(2×2,2,0) conv(40,3×3,1) relu maxpool(2×2,2,0) | conv(3,3×3,1) bn(3) relu maxpool(2×2,2,0) conv(16,3×3,1) relu maxpool(2×2,2,0) conv(32,3×3,1) relu maxpool(2×2,2,0) conv(64,3×3,1) relu maxpool(2×2,2,0) conv(128,3×3,1) relu maxpool(2×2,2,0) | conv(3,3×3,1) bn(3) relu maxpool(2×2,2,0) conv(20,3×3,1) relu maxpool(2×2,2,0) conv(40,3×3,1) relu maxpool(2×2,2,0) conv(80,3×3,1) relu maxpool(2×2,2,0) conv(100,3×3,1) relu maxpool(2×2,2,0) | conv(3,3×3,1) bn(3) relu maxpool(2×2,2,0) conv(10,3×3,1) relu maxpool(2×2,2,0) conv(20,3×3,1) relu maxpool(2×2,2,0) conv(40,3×3,1) relu maxpool(2×2,2,0) conv(80,3×3,1) relu maxpool(2×2,2,0) |
| fc(1024/10) | fc(512/10) | fc(640/10) | fc(320/10) | fc(256/10) | fc(320/10) | fc(160/10) | fc(128/10) | fc(100/10) | fc(80/10) |

TABLE XVI: Heterogeneous target networks (MNIST) having a common feature extractor and heterogeneous headers.

| CNN-1 | CNN-2 | CNN-3 | CNN-4 | CNN-5 | CNN-6 | CNN-7 | CNN-8 | CNN-9 | CNN-10 |
|--|--|--|--|--|--|--|--|--|--|
| conv(3,3×3,1) bn(3) relu maxpool(2×2,2,0) conv(16,3×3,1) bn(16) relu maxpool(2×2,2,0) | conv(3,3×3,1) bn(3) relu maxpool(2×2,2,0) conv(16,3×3,1) bn(16) relu maxpool(2×2,2,0) conv(32,3×3,1) bn(32) relu maxpool(2×2,2,0) | conv(3,3×3,1) bn(3) relu maxpool(2×2,2,0) conv(20,3×3,1) bn(20) relu maxpool(2×2,2,0) conv(40,3×3,1) bn(40) relu maxpool(2×2,2,0) | conv(3,3×3,1) bn(3) relu maxpool(2×2,2,0) conv(10,3×3,1) bn(10) relu maxpool(2×2,2,0) conv(20,3×3,1) bn(20) relu maxpool(2×2,2,0) | conv(3,3×3,1) bn(3) relu maxpool(2×2,2,0) conv(16,3×3,1) bn(16) relu maxpool(2×2,2,0) conv(32,3×3,1) bn(32) relu maxpool(2×2,2,0) conv(64,3×3,1) bn(64) relu maxpool(2×2,2,0) | conv(3,3×3,1) bn(3) relu maxpool(2×2,2,0) conv(20,3×3,1) bn(20) relu maxpool(2×2,2,0) conv(40,3×3,1) bn(40) relu maxpool(2×2,2,0) conv(80,3×3,1) bn(80) relu maxpool(2×2,2,0) | conv(3,3×3,1) bn(3) relu maxpool(2×2,2,0) conv(10,3×3,1) bn(10) relu maxpool(2×2,2,0) conv(20,3×3,1) bn(20) relu maxpool(2×2,2,0) conv(40,3×3,1) bn(40) relu maxpool(2×2,2,0) | conv(3,3×3,1) bn(3) relu maxpool(2×2,2,0) conv(16,3×3,1) bn(16) relu maxpool(2×2,2,0) conv(32,3×3,1) bn(32) relu maxpool(2×2,2,0) conv(64,3×3,1) bn(64) relu maxpool(2×2,2,0) conv(128,3×3,1) bn(128) relu maxpool(2×2,2,0) | conv(3,3×3,1) bn(3) relu maxpool(2×2,2,0) conv(20,3×3,1) bn(20) relu maxpool(2×2,2,0) conv(40,3×3,1) bn(40) relu maxpool(2×2,2,0) conv(80,3×3,1) bn(80) relu maxpool(2×2,2,0) conv(100,3×3,1) bn(100) relu maxpool(2×2,2,0) | conv(3,3×3,1) bn(3) relu maxpool(2×2,2,0) conv(10,3×3,1) bn(10) relu maxpool(2×2,2,0) conv(20,3×3,1) bn(20) relu maxpool(2×2,2,0) conv(40,3×3,1) bn(40) relu maxpool(2×2,2,0) conv(80,3×3,1) bn(80) relu maxpool(2×2,2,0) |
| fc(1024/10) | fc(512/10) | fc(640/10) | fc(320/10) | fc(256/10) | fc(320/10) | fc(160/10) | fc(128/10) | fc(100/10) | fc(80/10) |

TABLE XVII: Heterogeneous target networks (FMNIST and SVHN) having a common feature extractor and heterogeneous headers.

| CNN-1 | CNN-2 | CNN-3 | CNN-4 | CNN-5 | CNN-6 | CNN-7 | CNN-8 | CNN-9 | CNN-10 |
|--|--|--|--|--|--|--|--|--|--|
| conv(3,3×3,1) bn(3) relu conv(10,3×3,1) bn(10) relu maxpool(2×2,2,0) conv(16,3×3,1) relu maxpool(2×2,2,0) | conv(3,3×3,1) bn(3) relu conv(10,3×3,1) bn(10) relu maxpool(2×2,2,0) conv(16,3×3,1) bn(16) relu maxpool(2×2,2,0) conv(32,3×3,1) bn(32) relu maxpool(2×2,2,0) | conv(3,3×3,1) bn(3) relu conv(10,3×3,1) bn(10) relu maxpool(2×2,2,0) conv(20,3×3,1) bn(20) relu maxpool(2×2,2,0) conv(40,3×3,1) bn(40) relu maxpool(2×2,2,0) | conv(3,3×3,1) bn(3) relu conv(10,3×3,1) bn(10) relu maxpool(2×2,2,0) conv(20,3×3,1) bn(20) relu maxpool(2×2,2,0) conv(40,3×3,1) bn(40) relu maxpool(2×2,2,0) | conv(3,3×3,1) bn(3) relu conv(10,3×3,1) bn(10) relu maxpool(2×2,2,0) conv(20,3×3,1) bn(20) relu maxpool(2×2,2,0) conv(40,3×3,1) bn(40) relu maxpool(2×2,2,0) conv(80,3×3,1) bn(80) relu maxpool(2×2,2,0) | conv(3,3×3,1) bn(3) relu conv(10,3×3,1) bn(10) relu maxpool(2×2,2,0) conv(20,3×3,1) bn(20) relu maxpool(2×2,2,0) conv(40,3×3,1) bn(40) relu maxpool(2×2,2,0) conv(80,3×3,1) bn(80) relu maxpool(2×2,2,0) | conv(3,3×3,1) bn(3) relu conv(10,3×3,1) bn(10) relu maxpool(2×2,2,0) conv(20,3×3,1) bn(20) relu maxpool(2×2,2,0) conv(40,3×3,1) bn(40) relu maxpool(2×2,2,0) | conv(3,3×3,1) bn(3) relu conv(10,3×3,1) bn(10) relu maxpool(2×2,2,0) conv(16,3×3,1) bn(16) relu maxpool(2×2,2,0) conv(32,3×3,1) bn(32) relu maxpool(2×2,2,0) conv(64,3×3,1) bn(64) relu maxpool(2×2,2,0) conv(128,3×3,1) bn(128) relu maxpool(2×2,2,0) | conv(3,3×3,1) bn(3) relu conv(10,3×3,1) bn(10) relu maxpool(2×2,2,0) conv(20,3×3,1) bn(20) relu maxpool(2×2,2,0) conv(40,3×3,1) bn(40) relu maxpool(2×2,2,0) conv(80,3×3,1) bn(80) relu maxpool(2×2,2,0) conv(100,3×3,1) bn(100) relu maxpool(2×2,2,0) | conv(3,3×3,1) bn(3) relu conv(10,3×3,1) bn(10) relu maxpool(2×2,2,0) conv(20,3×3,1) bn(20) relu maxpool(2×2,2,0) conv(40,3×3,1) bn(40) relu maxpool(2×2,2,0) conv(80,3×3,1) bn(80) relu maxpool(2×2,2,0) |
| fc(1024/10) | fc(512/10) | fc(640/10) | fc(320/10) | fc(256/10) | fc(320/10) | fc(160/10) | fc(128/10) | fc(100/10) | fc(80/10) |

TABLE XVIII: Heterogeneous target networks (CIFAR10) having a common feature extractor and heterogeneous headers.

APPENDIX C
ADDITIONAL EXPERIMENT RESULTS

A. Different target networks

For the CIFAR10 dataset, we employed a diverse set of 10 heterogeneous target networks, comprising eight models with EfficientNet backbones (EfficientNet-B1 through EfficientNet-B7 [36]) and two models with ResNet backbones (ResNet18 and ResNet32 [35]). The hyperparameter settings for training the federated generative models are consistent with those outlined in Table X. As observed in Table XIX, similar to the results in Table IV, GEFL consistently outperforms the baseline methods. The performance degradation observed in both the baselines and GEFL can be attributed to the increased training demands, requiring more communication rounds and larger volumes of data to effectively train the target networks, particularly for larger models such as EfficientNet and ResNet.

| Method | FedAvg | GEFL (FedDCGAN) |
|-------------|------------------|-------------------------|
| None | 45.11 \pm 0.46 | 50.43 \pm 1.01 |
| MixUp | 47.99 \pm 3.15 | 52.95 \pm 0.78 |
| CutMix | 46.61 \pm 1.29 | 51.21 \pm 1.09 |
| AugMix | 45.18 \pm 0.92 | 51.76 \pm 0.92 |
| AutoAugment | 47.89 \pm 0.21 | 51.77 \pm 2.03 |

TABLE XIX: Mean classification accuracy (%) comparison to data augmentation on Res+Eff target networks. GEFL outperforms other baselines and is effective combined with data augmentation.

B. Memorization of generative models

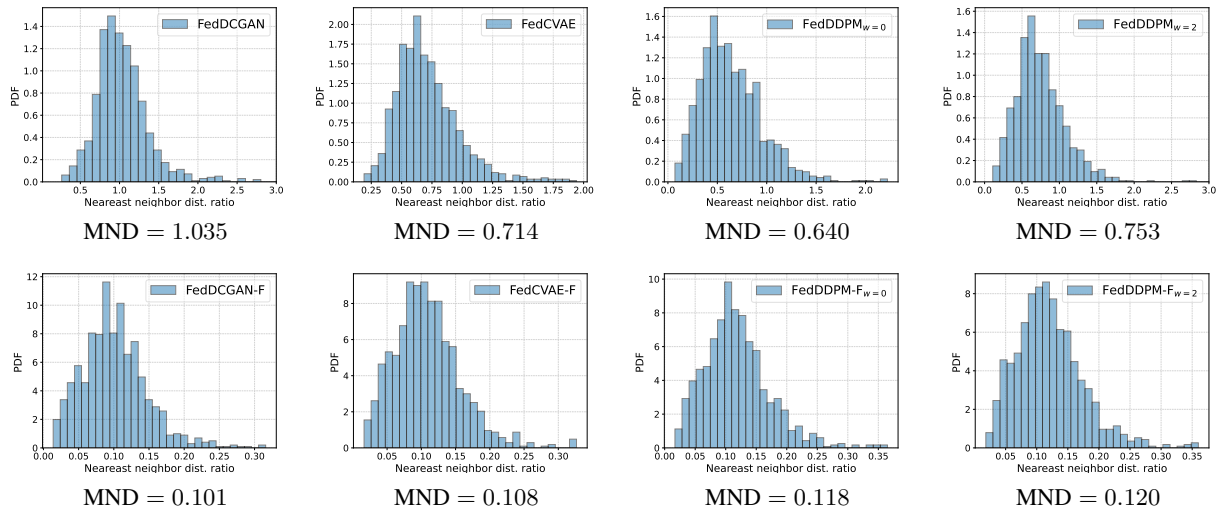


Fig. 11: Memorization analysis of generative models and feature-generative models in GEFL and GEFL-F, respectively, assessed through the MND ratio on MNIST dataset. Here, the x-axis and y-axis represent the nearest neighbor distance ratio and the distribution over training set, respectively.

We measure privacy in our framework, GEFL and GEFL-F, in terms of *memorization*. In GEFL, where the target networks are not shared, privacy leakage is solely due to the memorization of shared generative models. Memorization occurs when there is an increased probability of generating a sample closely resembling the training data [53]. This is particularly concerning in scenarios involving sensitive data like medical images or images containing private information. A typical way to evaluate memorization is to compare the generated samples to their nearest neighbors in the training set [54], [79].

We elaborated on how we assess memorization in GEFL using the *mean nearest neighbor distance (MND) ratio*, as detailed in Section III-C. The MND ratio for each training sample is computed as the ratio between the distance to the nearest synthetic sample and the nearest validation sample. While any metric can be employed as a distance [53], we use the perceptual metric LPIPS, which captures image similarity as human perception, in contrast to traditional metrics like Euclidean distance. The memorization of federated generative models of GEFL is evaluated as Figure 11, illustrating the distribution of the nearest neighbor distance ratio over the training set of MNIST.

In GEFL-F, a common feature extractor and feature-generative model are shared between the server and clients in the FL pipeline. A promising way that attacker can take using trained feature extractor and feature-generative model is to generated

synthetic features from generative model and apply model inversion using feature extractor. To evaluate the vulnerability of GEFL-F in such scenario, we assume a white-box feature extractor and apply model inversion [51] using generated features to get reconstructed images as Figure 5. Subsequently, we compare the original real images with the reconstructed ones by measuring the MND ratio, as we did in GEFL. In Figure 11, it is observed that incorporating feature-generative models mitigates privacy preservation compared to GEFL, even though it shares a common feature extractor.

C. Guidance score and time steps of diffusion models

We present additional results analyzing the impact of the guidance score on performance, with a particular focus on its correlation with time steps T . By varying the time steps for DDPM, we observed that under sufficient time steps, lower guidance scores ($w = 0$) yielded superior performance compared to higher guidance scores ($w = 2$), as shown in Table XX. Within our framework, while lower guidance scores enhance sample diversity, using fewer time steps results in degraded image quality, leading to better performance with higher guidance scores under such conditions.

| T | 30 | 60 | 100 | T | 30 | 60 | 100 |
|---------|-------------------------|-------------------------|-------------------------|---------|-------------------------|-------------------------|-------------------------|
| $w = 0$ | 94.79 \pm 0.37 | 95.68 \pm 0.32 | 96.44 \pm 0.05 | $w = 0$ | 80.49 \pm 1.29 | 81.72 \pm 0.09 | 82.43 \pm 0.22 |
| $w = 2$ | 95.18 \pm 0.14 | 95.60 \pm 0.16 | 95.17 \pm 0.14 | $w = 2$ | 82.08 \pm 0.35 | 81.87 \pm 0.43 | 81.51 \pm 0.38 |

(a) MNIST
(b) FMNIST

TABLE XX: Mean accuracy (%) of GEFL with FedDDPM across different guidance scores and time steps T .

APPENDIX D
EXAMPLE OF GENERATED SAMPLES AND FEATURES

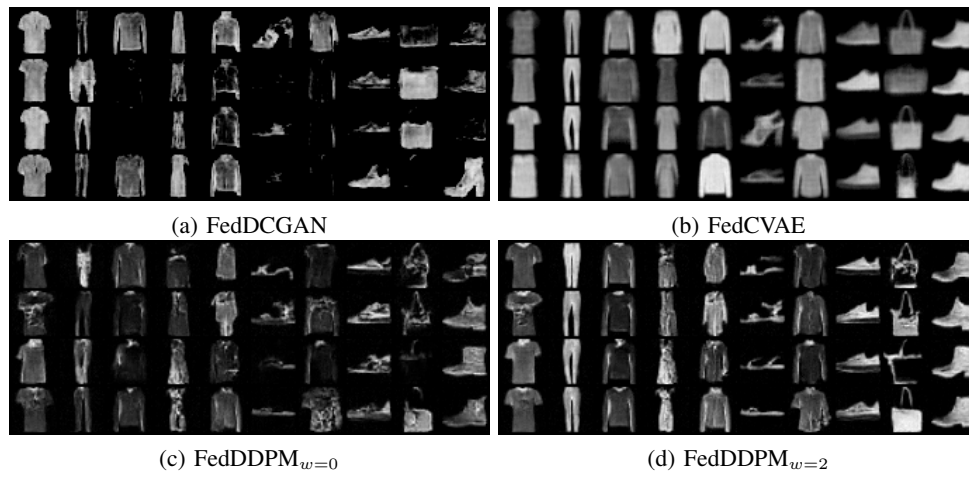


Fig. 12: **Generated samples of FMNIST** by federated generative models with 10 clients in GEFL.

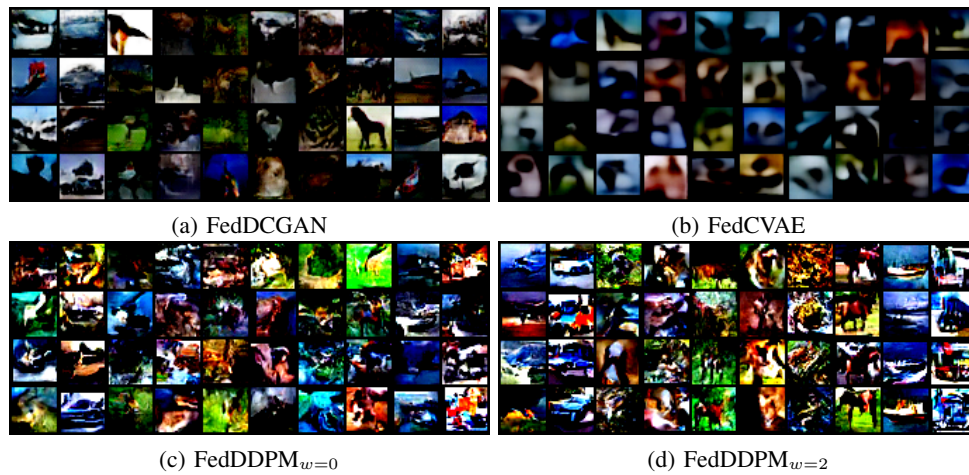


Fig. 13: **Generated samples of CIFAR10** by federated generative models with 10 clients in GEFL.

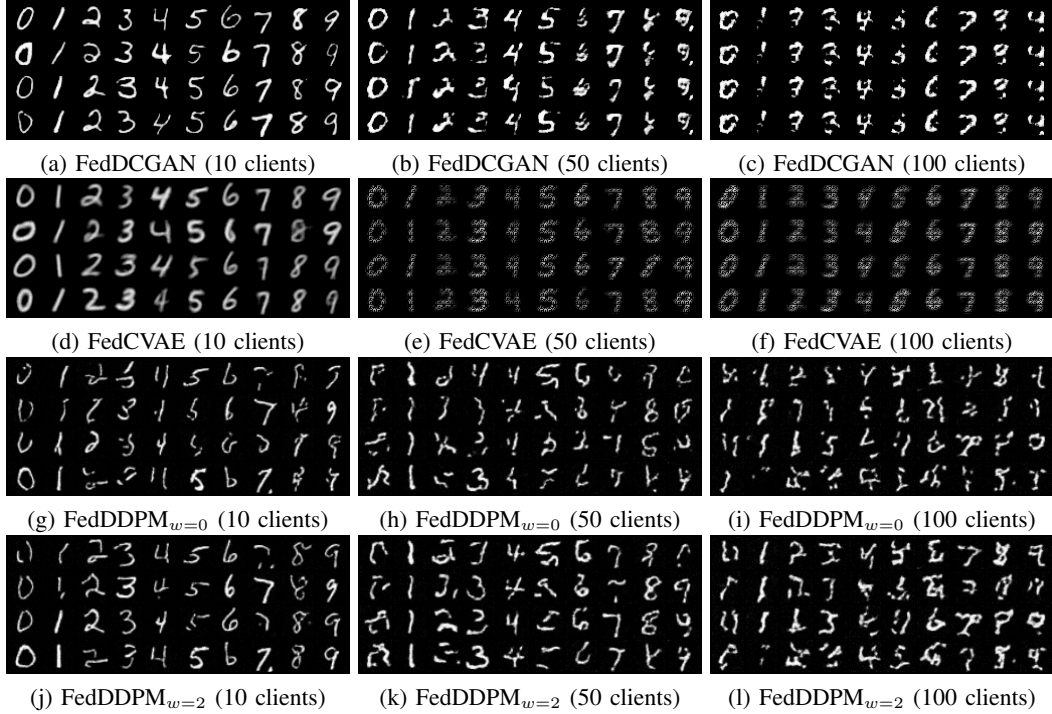


Fig. 14: Generated samples of MNIST by federated generative models in GEFL across the different number of users.

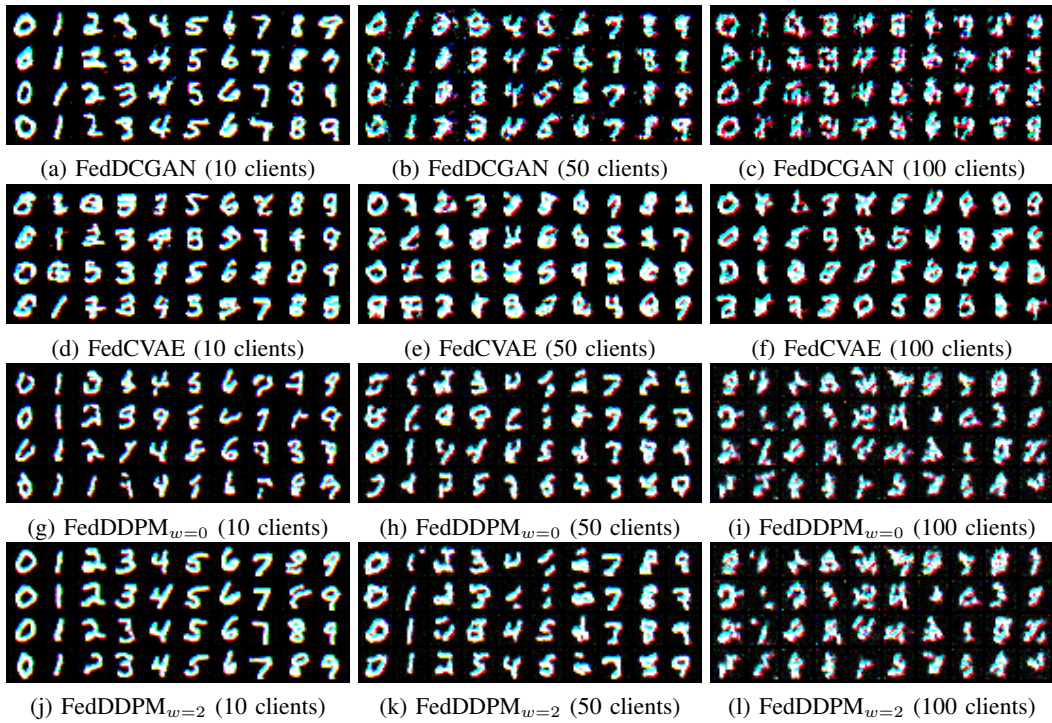


Fig. 15: Feature samples of MNIST generated by feature-generative models in GEFL-F across the different number of users.